The EMTO method
Fundamentals, implementation and demonstration

Levente Vitos

Applied Materials Physics, Department of Materials Science and Engineering,
Royal Institute of Technology Stockholm

NAISS/ENCCS VASP/EMTO Best Practices Workshop
16/4/2024

Collaboration

Hans L. Skriver (1998-2000)

Wei Li

Andreas Östlin

Henrik Levämäki

The EMTO theory

Exact muffin-tin orbital theory

Andersen O. K., Jepsen O., Krier G.

1994

in: Lectures on Methods of Electronic Structure Calculations, eds.: V. Kumar, O. K. Andersen, A. Mookerjee. Singapore, World Scientific.

NMTO

Andersen O. K., Saha-Dasupta, T.

Phys. Rev. B 62, R16219 (2000)

What is “exact” in the EMTO method?

PRB Referee report (2004):

“…*The use of the term “exact” in connection with the EMTO label I find inappropriate and unfortunate, although I recognize that by this time it is written in stone. No significant aspect of any modern band structure method is exact…”*

The Schrödinger equation is solved “exactly” for the MT potential

- “exact” kinetic energy
- “exact” charge density

Density Functional Theory

Consider a system of N interacting electrons. The total energy is:

$$E_e = T + E_{ee} + E_{en} + E_{nn}$$

Total energy is a functional of the electron density n(r)

P.C. Hohenberg

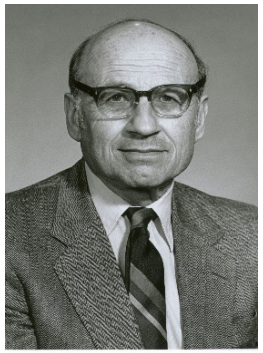

W. Kohn

1964

$$E_e = E[n]$$

where $\int n(r)dr = N$

all trial densities should contain the same number of electrons

Minimizing the total energy functional

- *We should plug in all possible n(r) in E[n]*
- *n(r) should be consistent with the number of electrons*
- *search until we find the minimum of E[n]*

$$\min_{n} E[n] = E_0$$

=> Schrödinger equation is solved!

In practice this route based on variational principle is not feasible because we do not know the exact form of E[n]

DFT-level approximations are needed!

Restructuring the total energy functional

We separate the known parts of E[n]

$$E[n] = T_s[n] + \frac{1}{2}\int v_H([n];r)n(r)dr + \int v_e([n];r)n(r)dr + E_{xc}[n]$$

known terms (large terms)

$T_s[n]$ **kinetic energy of non-interacting electrons**

$$v_H([n];r) = 2\int \frac{n(r')}{|r-r'|}dr'$$ **Hartree potential**

$$v_e(r) = -\sum_R \frac{2Z_R}{|r-R|}$$ **external potential**

and the rest (small terms)

$E_{xc}[n]$ **exchange-correlation energy**

From the original interacting system to the non-interacting model system

Interacting electrons in external potential:
(original many-body problem)

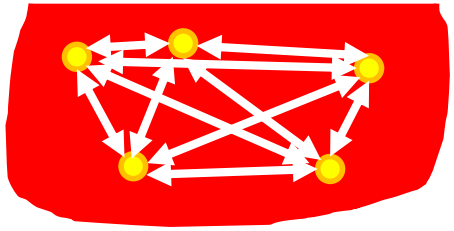

$V_e([n];r)$

$$E[n] = T_s[n] + \frac{1}{2}\int v_H([n];r)n(r)dr + \int v_e([n];r)n(r)dr + E_{xc}[n]$$

Non-interacting electrons moving in an effective potential:
Note: the potential involves the **functional derivative** of the xc energy

$$E[n] = T_s[n] + \int v([n];r)n(r)dr$$

$$v([n];r) = v_e(r) + v_H([n];r) + \frac{\delta E_{xc}[n]}{\delta n(r)}$$

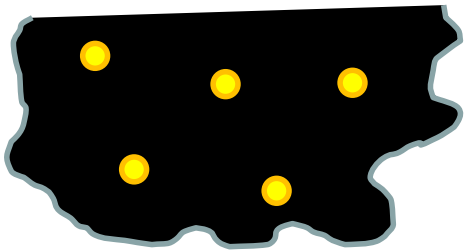

$V([n];r)$

Kohn-Sham equations

We can solve the non-interacting system ***which by construction leads to the same density as the real system***

$$\{-\nabla^2 + v([n];r)\}\Psi_j(r) = \varepsilon_j \Psi_j(r)$$

In KS scheme, the wave function depends only on the position of one single electron

Self consistent solution:

input = output

$$n(r) = \sum_{\varepsilon_j \le \varepsilon_F} |\Psi_j(r)|^2$$

Compare with Schrödinger eq.

$$\hat{H}\Psi_k = E_k \Psi_k$$

$$\Psi_k(\mathbf{r}_1, \mathbf{r}_2, \ldots, \mathbf{r}_N)$$

Effective potential:

$$v([n];r) = v_e(r) + v_H([n];r) + \frac{\delta E_{xc}[n]}{\delta n(r)}$$

Solving the Kohn-Sham single-electron equations

$$\left(-\frac{\nabla^2}{2}+V_{eff}(\mathbf{r})\right)\psi_p(\mathbf{r})=\varepsilon_p\psi_p(\mathbf{r})$$

Two methods to get Kohn-Sham orbitals:

1. Solve Kohn-Sham equation *directly* on a real-space grid (grid methods).

2. Use some basis functions for representation of Kohn-Sham orbitals:

$$\psi_p(\mathbf{r})=\sum_i C_{pi}\varphi_i; \qquad \varphi_i \text{ are basis functions}$$

The choice of the basis functions in principle does not matter for the final result, however, if it is done in a clever way, it makes calculations efficient.

The great variety of first-principles methods is about this point: optimization of the basis. Our computers are not powerful enough even to solve accurately Kohn-Sham equations without using special numerical tricks.

Variational principle for the Kohn-Sham equation

$$\delta\left[\langle\psi|H|\psi\rangle - E\left(\langle\psi|\psi\rangle - N\right)\right]\Big/\delta\psi = 0$$

$$\psi = \sum_i c_i\varphi_i \qquad \langle\psi|H|\psi\rangle = \sum_{ij} c_i^* c_j H_{ij} \quad \text{where } H_{ij} = \int d\mathbf{r}\,\varphi_i^*(\mathbf{r}) H \varphi_j(\mathbf{r})$$

In general (if the basis functions are not orthonormal):

$$\langle\psi|\psi\rangle = \sum_{ij} c_i^* c_j S_{ij} \quad \text{where } \mathrm{S}_{ij} = \int d\mathbf{r}\,\varphi_i^*(\mathbf{r})\varphi_j(\mathbf{r})$$

it is called overlap matrix

Here, c_i are the coefficients to be found.

$$\delta\left[\sum_{ij} c_i^* c_j H_{ij} - \varepsilon \sum_{ij} c_i^* c_j S_{ij}\right]\Big/\delta c_i^* = 0$$

$$\sum_j c_j\left(H_{ij} - \varepsilon S_{ij}\right) = 0$$

This is a homogeneous set of linear equations for c and ε

It has non-trivial (not 0) solutions only if the determinant vanishes:

This equation gives the one electron energies (ε)

$$\det\left[\mathbf{H} - \varepsilon\mathbf{S}\right] = 0$$

The EMTO method, Implementation (1998-2001)

The EMTO formalism

The KS potential is approximated by the overlapping optimized muffin-tin potential

$$v(\mathbf{r}) \approx v_{mt}(\mathbf{r}) \equiv v_0 + \sum_R [v_R(r_R) - v_0]$$

$v_R(r_R)$ is spherical for $r_R \leq S_R$ and
$v_R(r_R) = v_0$ for $r_R > S_R$
v_0 is the constant potential connecting the local potential wells

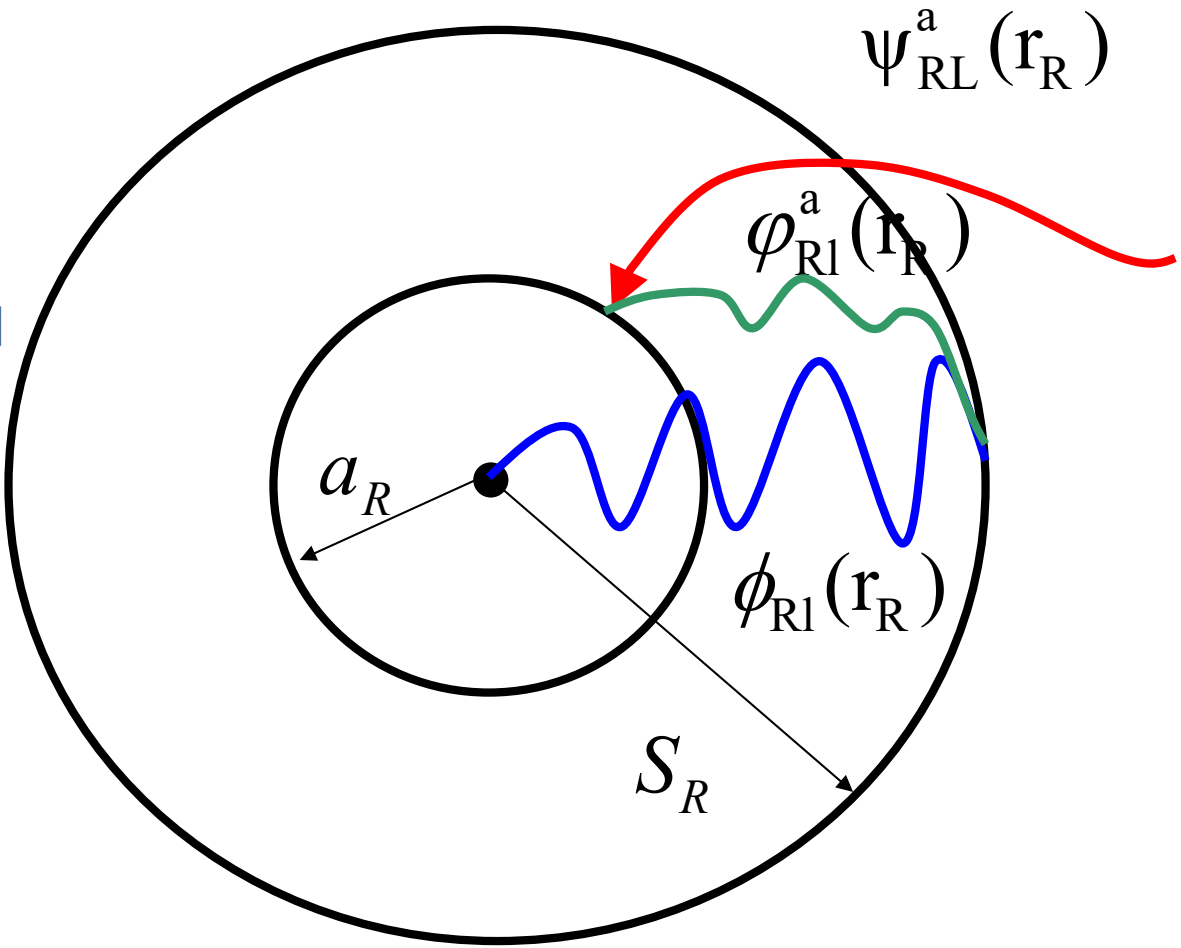

$\psi^a_{RL}(r_R)$

Screened spherical wave (constant potential)

$\varphi^a_{Rl}(r_R)$

Local free electron solution (constant potential)

$\phi_{Rl}(r_R)$

Partial wave (solution of the spherical Schrödinger eq.)

The screened spherical waves; $S^a_{R'L'RL}$

Solutions for the constant potential (Bessel and Neumann functions):

$$\left\{\nabla^2 + \kappa^2\right\} \psi^a_{RL}(\kappa^2, \mathbf{r}_R) = 0, \qquad \kappa^2 \equiv \epsilon - v_0.$$

Screening is realized with "hard" spheres of radius a_R:

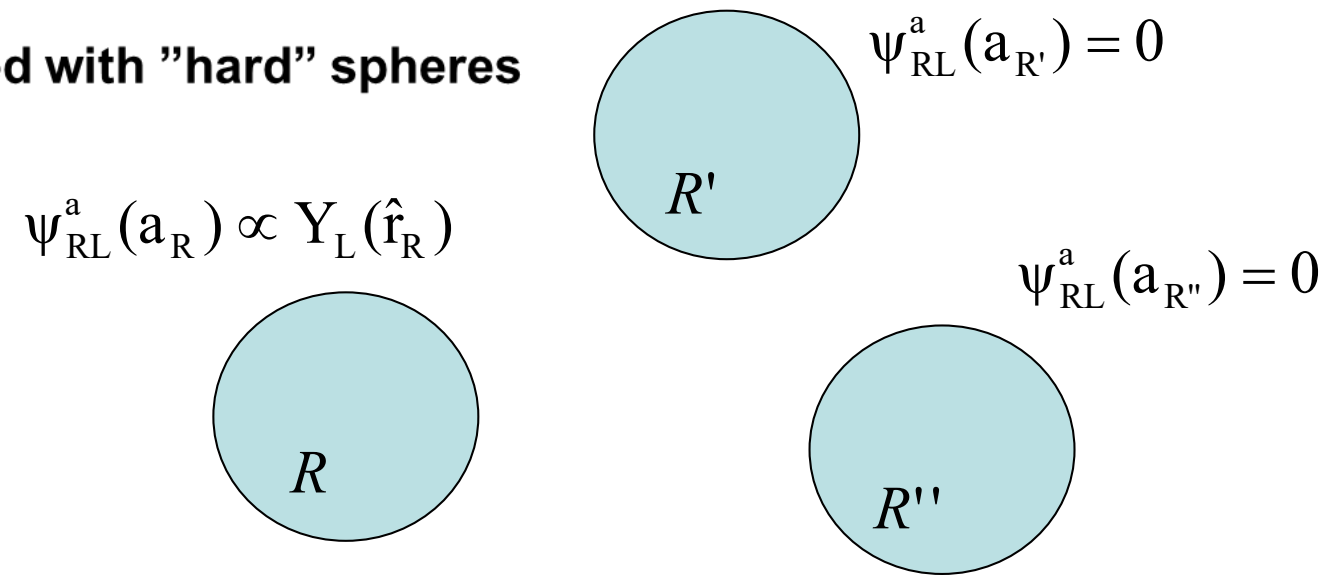

Boundary conditions require a multi-center form:

$$\psi^a_{RL}(\kappa^2, \mathbf{r}_R) = f^a_{Rl}(\kappa^2, r_R)\, Y_L(\hat{r}_R)\delta_{RR'}\, \delta_{LL'} + \sum_{L'} g^a_{R'l'}(\kappa^2, r_{R'})\, Y_{L'}(\hat{r}_{R'})\, S^a_{R'L'RL}(\kappa^2).$$

The screened spherical waves

$$\psi^a_{RL}(\kappa^2, \mathbf{r}_R) = f^a_{Rl}(\kappa^2, r_R)\, Y_L(\hat{r}_R)\delta_{RR'}\, \delta_{LL'} + \sum_{L'} g^a_{R'l'}(\kappa^2, r_{R'})\, Y_{L'}(\hat{r}_{R'})\, S^a_{R'L'RL}(\kappa^2).$$

$$f^a_{Rl}(\kappa^2, r)|_{a_R} = 1 \text{ and } g^a_{Rl}(\kappa^2, r)|_{a_R} = 0.$$

$$\left.\frac{\partial f^a_R(\kappa^2, r)}{\partial r}\right|_{a_R} = 0 \text{ and } \left.\frac{\partial g^a_{Rl}(\kappa^2, r)}{\partial r}\right|_{a_R} = \frac{1}{a_R}.$$

Linear combinations of the Bessel and Neumann functions:

$$f^a_{Rl}(\kappa^2, r) = t^1_{Rl}(\kappa^2) n_l(\kappa^2, r) + t^2_{Rl}(\kappa^2) j_l(\kappa^2, r)$$

$$g^a_{Rl}(\kappa^2, r) = -t^3_{Rl}(\kappa^2) n_l(\kappa^2, r) - t^4_{Rl}(\kappa^2) j_l(\kappa^2, r).$$

Screening matrix:

$$\left\{ \begin{matrix} t^1_{Rl}(\kappa^2) & t^2_{Rl}(\kappa^2) \\ t^3_{Rl}(\kappa^2) & t^4_{Rl}(\kappa^2) \end{matrix} \right\} = 2\frac{a_R^2}{w} \left\{ \begin{matrix} \frac{\partial j_l(\kappa^2, a_R)}{\partial r_R} & -\frac{\partial n_l(\kappa^2, a_R)}{\partial r_R} \\ \frac{1}{a_R} j_l(\kappa^2, a_R) & -\frac{1}{a_R} n_l(\kappa^2, a_R) \end{matrix} \right\}.$$

The local free electron solution

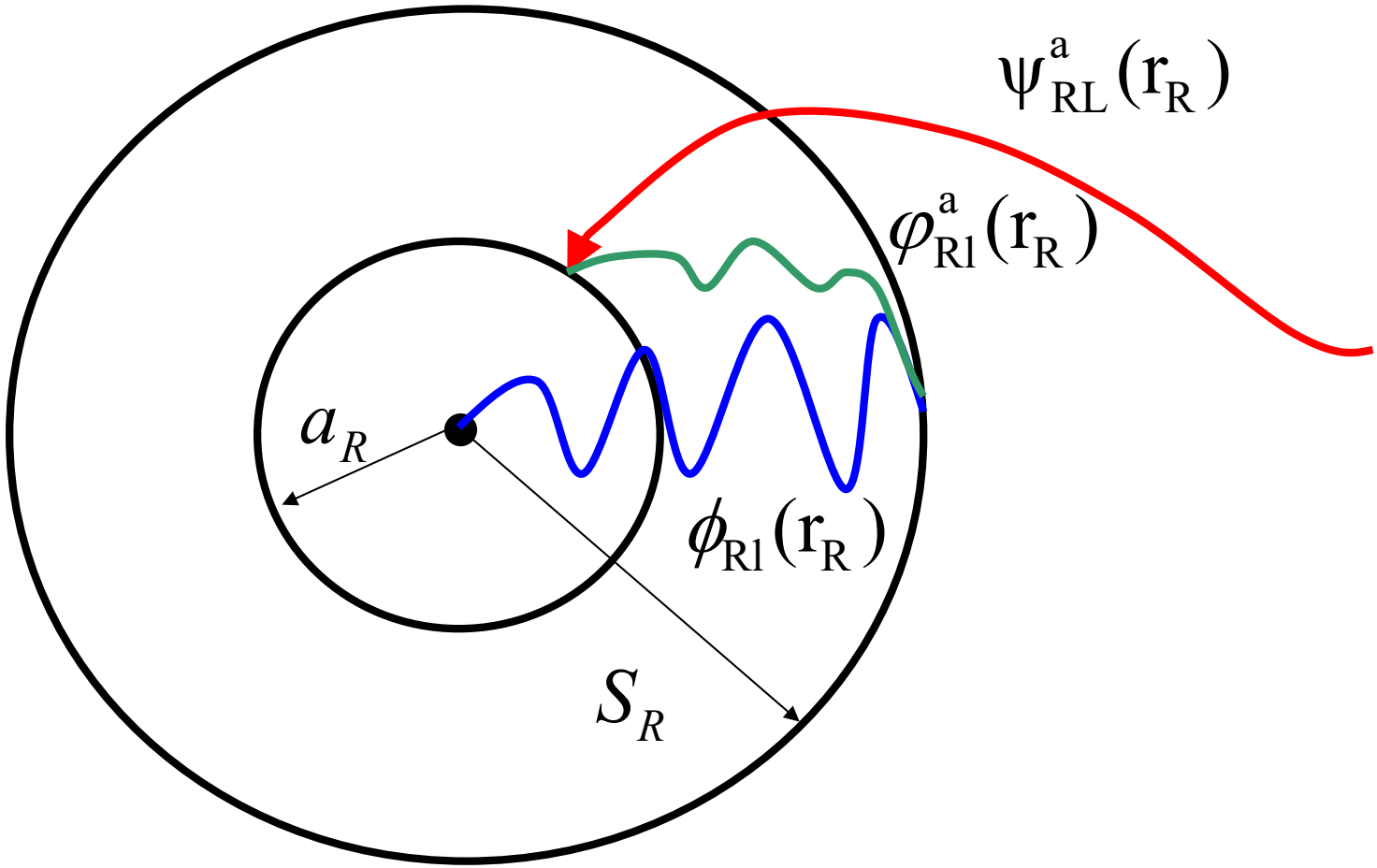

$$\varphi^a_{Rl}(\epsilon, r_R) = f^a_{Rl}(\kappa^2, r_R) + g^a_{Rl}(\kappa^2, r_R)\, D^a_{Rl}(\epsilon),$$

By construction, it joins the screened spherical wave at a_R
There is a slope difference (first order derivative is discontinuous).

Partial wave; D_{Rl}^{a}

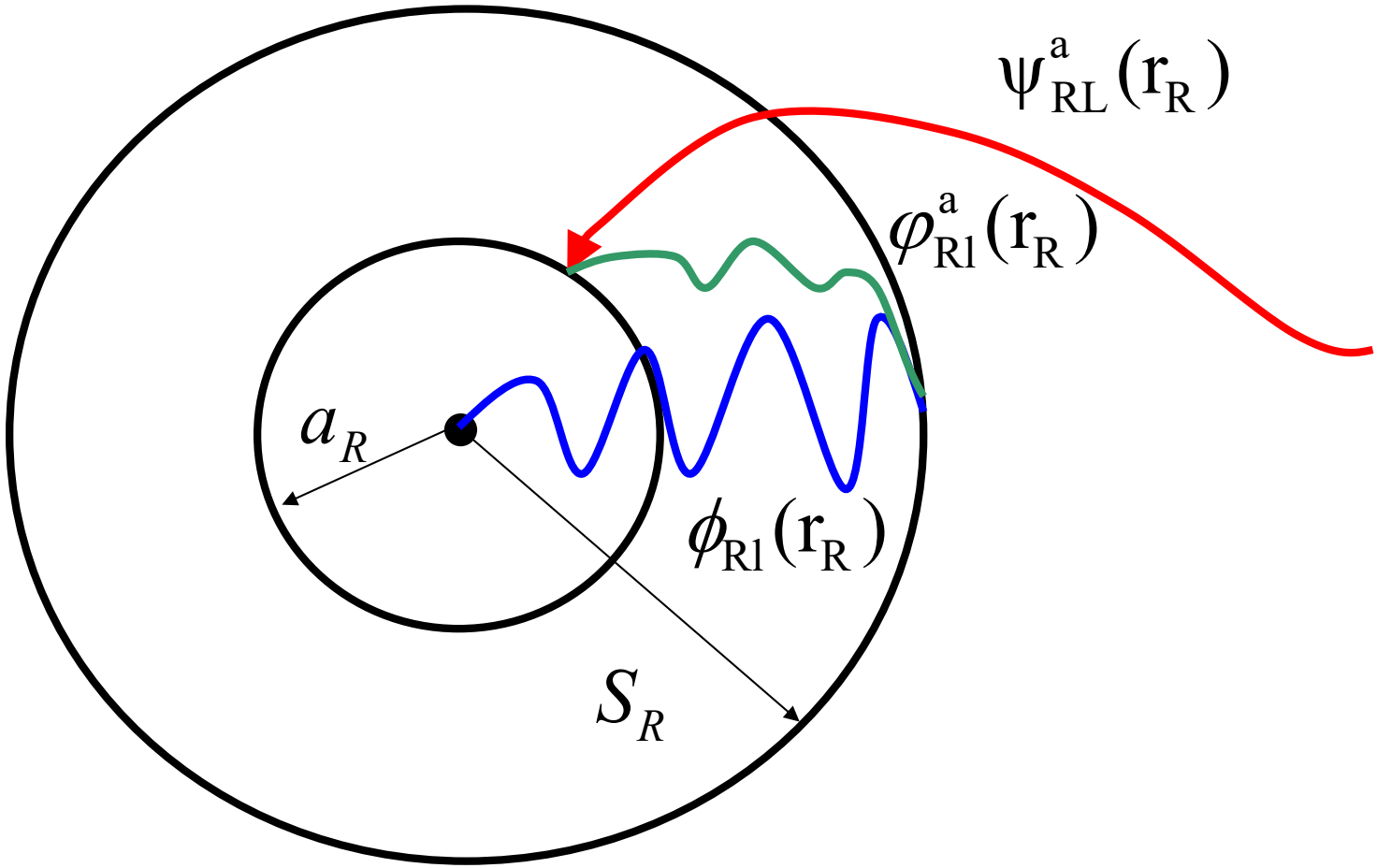

It is the solution of the radial Schrodinger equation for $r_R \leq S_R$, potential $v_R(r_R)$.
It joins continuously the local free electron solution at S_R.
This condition gives the slope of the local free electron solution at a_R (D_{Rl}^{a}).

The kink cancellation condition

The Exact Muffin-Tin Orbitals:

$$\bar{\psi}^a_{RL}(\epsilon, \mathbf{r}_R) = \psi^a_{RL}(\kappa^2, \mathbf{r}_R) + N^a_{Rl}(\epsilon)\, \phi_{Rl}(\epsilon, r_R)\, Y_L(\hat{r}_R) - \varphi^a_{Rl}(\epsilon, r_R)\, Y_L(\hat{r}_R),$$

$$\Psi(\mathbf{r}_R) = \sum_L N^a_{Rl}(\epsilon)\, \phi_{Rl}(\epsilon, r_R)\, Y_L(\hat{r}_R)\, v^a_{RL} + \sum_L \left[f^a_{Rl}(\kappa^2, r_R) v^a_{RL} + g^a_{Rl}(\kappa^2, r_R) \sum_{R'L'} S^a_{RL\,R'L'}(\kappa^2) v^a_{R'L'} \right] Y_L(\hat{r}_R) - \sum_L \left[f^a_{Rl}(\kappa^2, r_R) + g^a_{Rl}(\kappa^2, r_R) D^a_{Rl}(\epsilon) \right] Y_L(\hat{r}_R)\, v^a_{RL}. \quad (2.29)$$

It is solution for the full Schrödinger equation if the second and third terms vanish:

$$\sum_{RL} a_{R'} \left[S^a_{R'L'RL}(\kappa_j^2) - \delta_{R'R}\delta_{L'L}\, D^a_{Rl}(\epsilon_j) \right] v^a_{RL,j} = 0,$$

Overlap matrix :

$$\int \bar{\psi}^*_{R'L'}(\epsilon, \mathbf{r})\, \bar{\psi}_{RL}(\epsilon, \mathbf{r})\, d\mathbf{r} = a_R \dot{S}^a_{R'L'RL}(\kappa^2) - a_R \dot{D}^a_{Rl}(\epsilon) = \dot{K}^a_{R'L'RL}(\epsilon).$$

Slope matrix

$$\kappa^2 \equiv \epsilon - v_0,$$

$$S^a_{R'L'RL} = \frac{t^1_{Rl}}{t^3_{Rl}}\delta_{R'R}\delta_{L'L} + \frac{1}{t^3_{R'l'}}\left[-S^0 - \frac{t^4_{Rl}}{t^3_{Rl}}\right]^{-1}_{R'L'RL}\frac{d^a_{Rl}}{t^3_{Rl}},$$

$$n_L(\kappa^2, \mathbf{r}_R) = -\sum_{L'} j_{L'}(\kappa^2, \mathbf{r}_{R'})\, S^0_{R'L'RL}(\kappa^2).$$

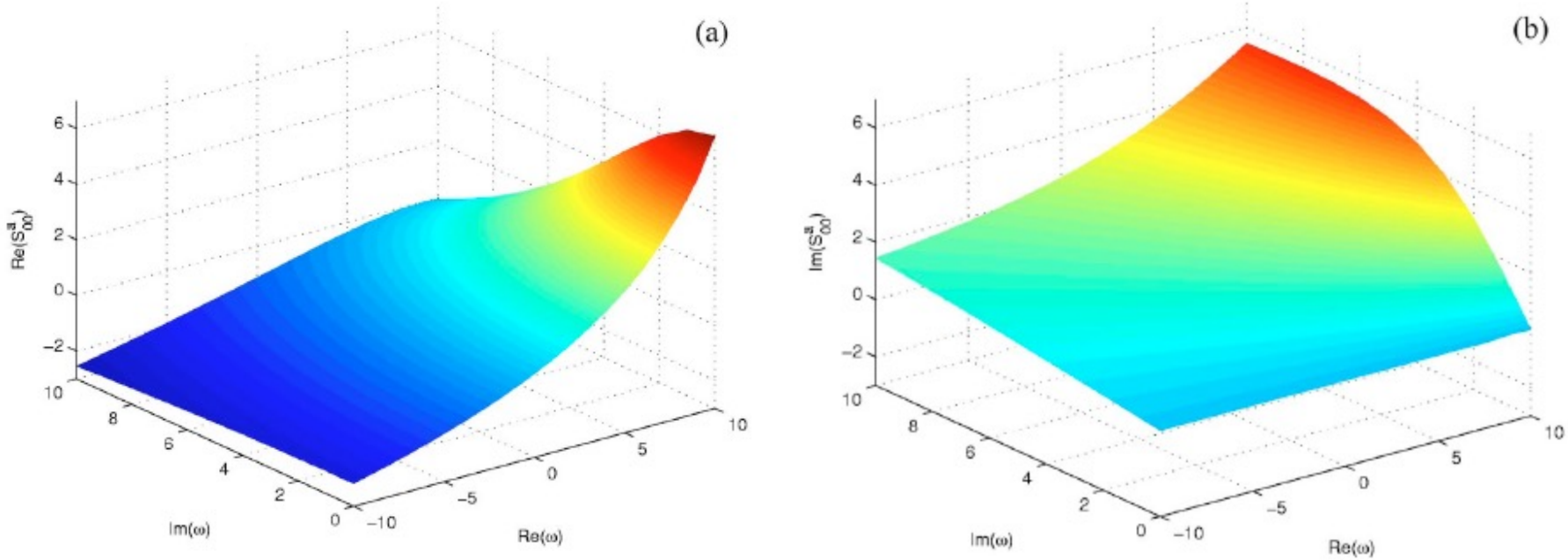

The effect of the hard (screening) sphere radius

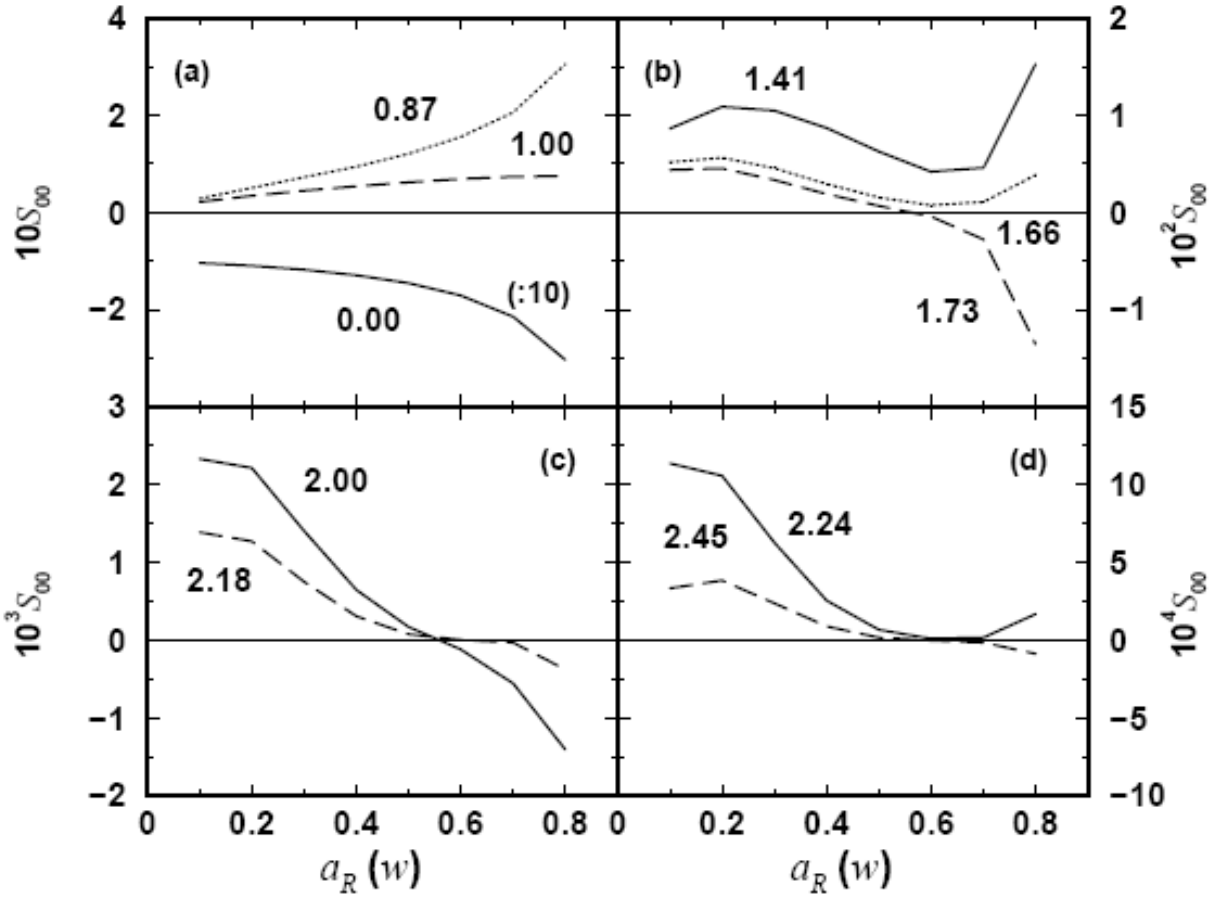

Fig. 3.1. The *ss* element of the *bcc* slope matrix for $\omega = 0$ plotted as a function of the hard sphere radius a_R and the radius of the coordination shell $d_{R'R}$ (shown by numbers in units of lattice constant). Note that in panel (a), the scale for $d_{R'R} = 0.00a$ has been divided by 10.

Parametrization of the slope matrix

$$S^a(\omega) \approx S^a_n(\omega;\omega_0) \equiv S^a(\omega_0) + \frac{1}{1!}\frac{dS^a(\omega)}{d\omega}(\omega-\omega_0)$$

$$+ \frac{1}{2!}\frac{d^2S^a(\omega)}{d\omega^2}(\omega-\omega_0)^2 + \cdots + \frac{1}{n!}\frac{d^nS^a(\omega)}{d\omega^n}(\omega-\omega_0)^n.$$

$$\kappa^2 \equiv \epsilon - v_0,$$

$$\omega \equiv (\kappa w)^2$$

Slope matrix and first derivative (3rd order single-center expansion)

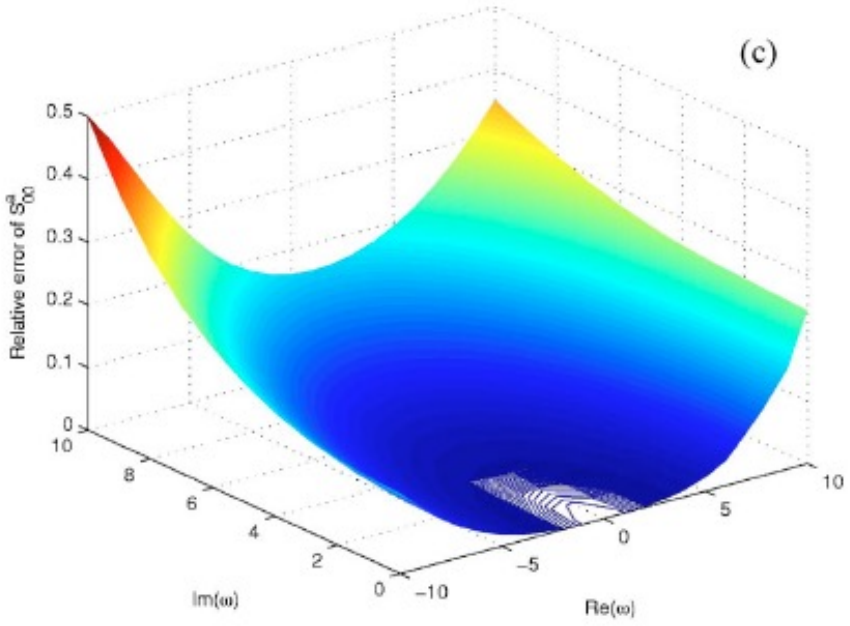

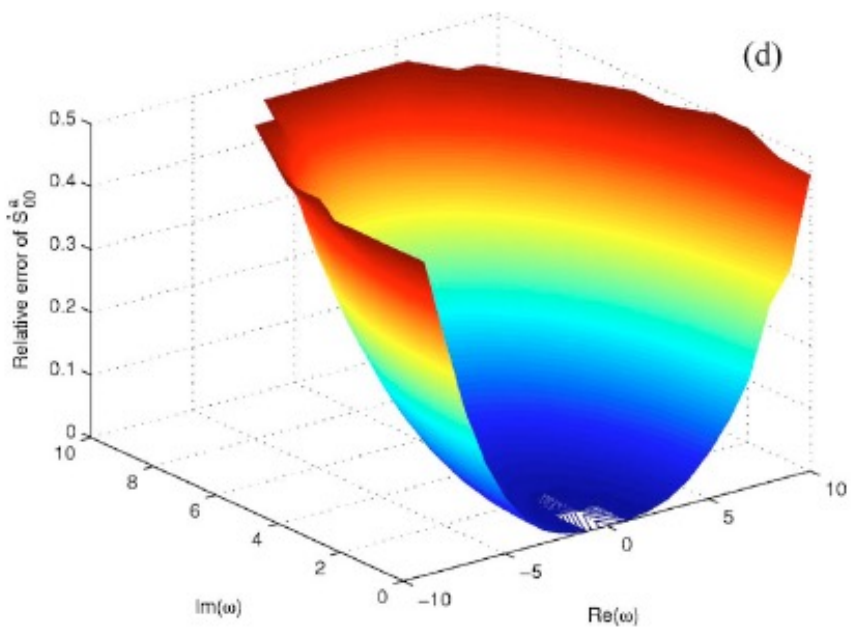

Parametrization of the slope matrix

$$S^a(\omega) \approx S^a_n(\omega;\omega_0) \equiv S^a(\omega_0) + \frac{1}{1!}\frac{dS^a(\omega)}{d\omega}(\omega-\omega_0)$$

$$+\frac{1}{2!}\frac{d^2S^a(\omega)}{d\omega^2}(\omega-\omega_0)^2 + \cdots + \frac{1}{n!}\frac{d^nS^a(\omega)}{d\omega^n}(\omega-\omega_0)^n. \qquad \omega \equiv (\kappa w)^2$$

Slope matrix and first derivative (6th order single-center expansion)

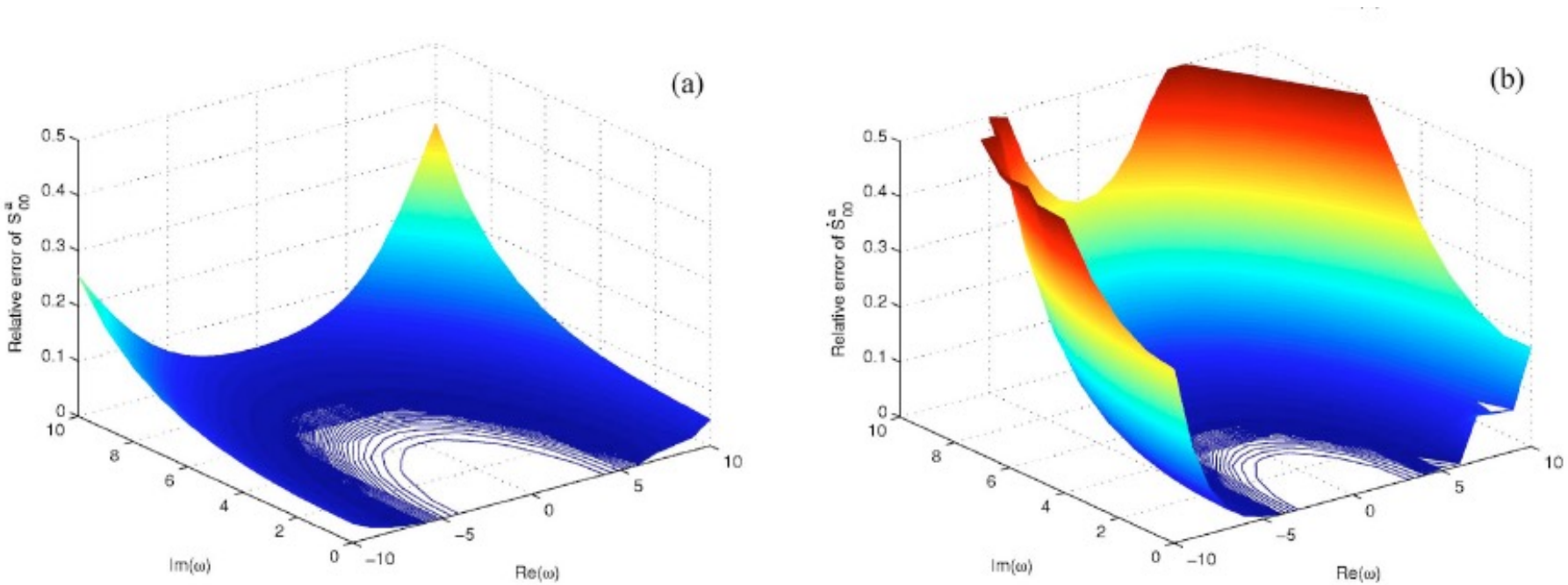

Parametrization of the slope matrix

$$S^a(\omega) \approx S^a_{n,m}(\omega;\omega_1,\omega_2) = S^a_n(\omega;\omega_1) + \frac{1}{(n+1)!}a_{n+1}(\omega-\omega_1)^{n+1} + \cdots + \frac{1}{(n+m)!}a_{n+m+1}(\omega-\omega_1)^{n+m+1},$$

$$S^a_{n,m}(\omega_2;\omega_1,\omega_2) = S^a(\omega_2),$$

$$\left.\frac{dS^a_{n,m}(\omega;\omega_1,\omega_2)}{d\omega}\right|_{\omega=\omega_2} = \left.\frac{dS^a(\omega)}{d\omega}\right|_{\omega=\omega_2}, \ldots$$

$$\left.\frac{d^mS^a_{n,m}(\omega;\omega_1,\omega_2)}{d\omega^m}\right|_{\omega=\omega_2} = \left.\frac{d^mS^a(\omega)}{d\omega^m}\right|_{\omega=\omega_2}.$$

Slope matrix and first derivative (6+6th order two-center expansion)

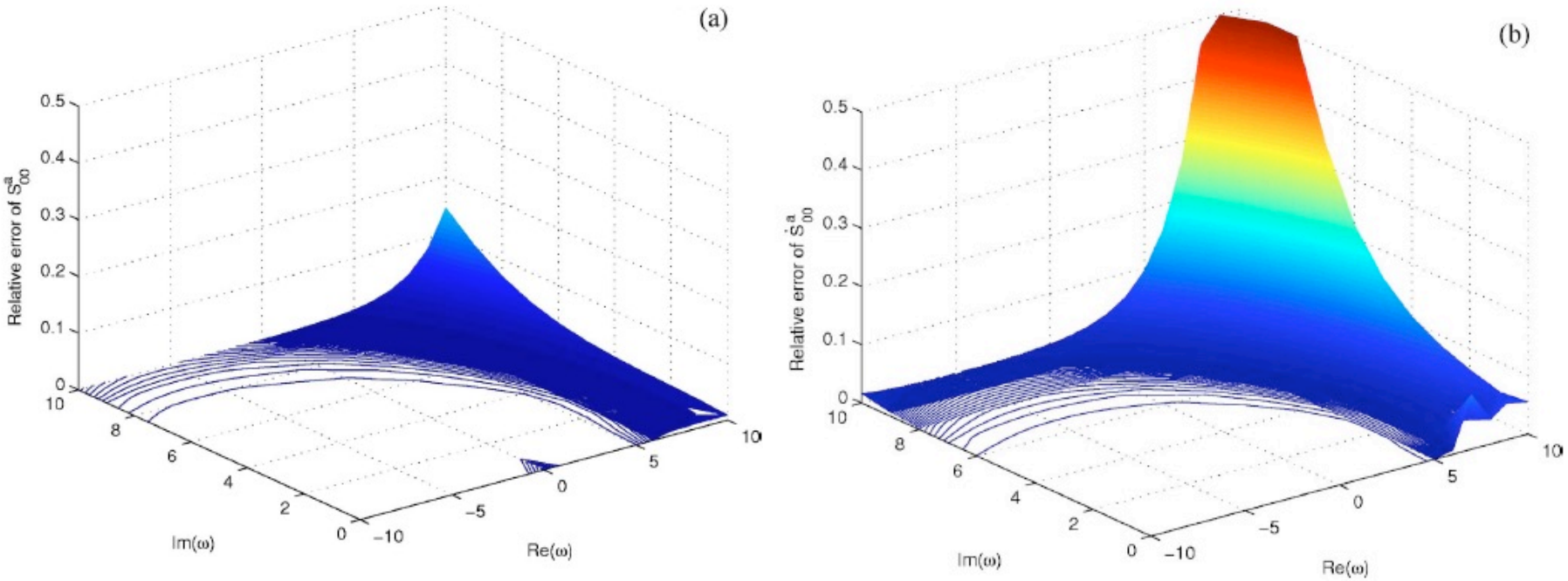

Accuracy: slope matrix and charge density

$$\Delta_e(l^h_{max}) = \sum_R \int_{\Omega_R} n(\mathbf{r}_R) d\mathbf{r}_R - N_e$$

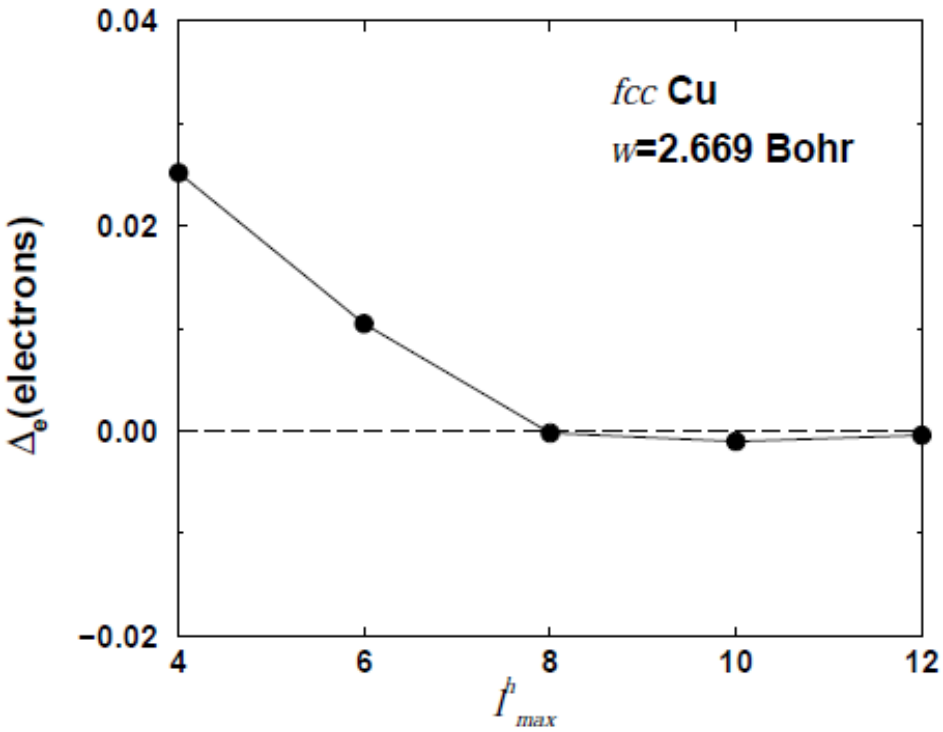

Fig. 4.7. The calculated charge misfit Δ_e for *fcc* Cu plotted as a function of l^h_{max}.

Optimized Overlapping Muffin-Tin potential

O. K. Andersen, et al. (1994)

$$v_{FP}(\mathbf{r}) \cong v_{mt}(\mathbf{r})$$

$$v_{mt}(\mathbf{r}) = v_0 + \Sigma_R [v_R(r_R) - v_0]$$

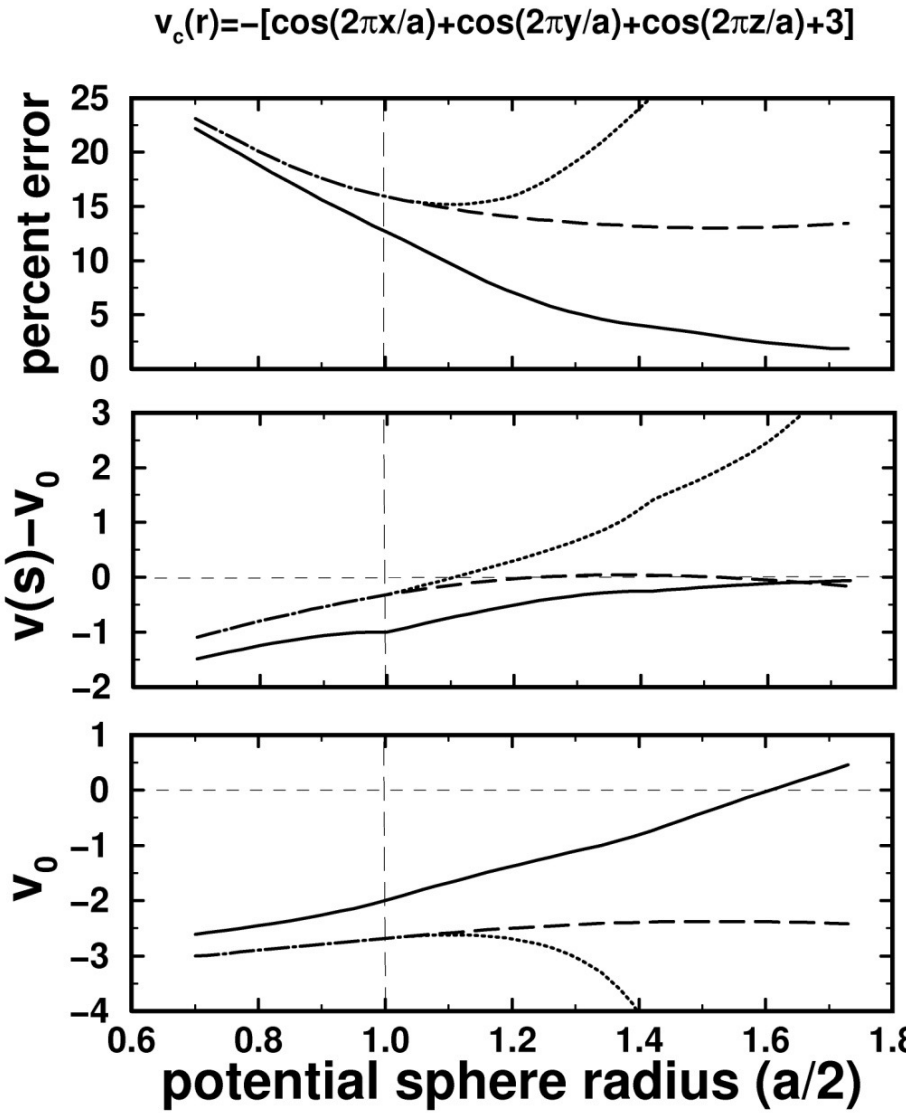

Optimized Overlapping Muffin-Tin potential Examples: Fe-C

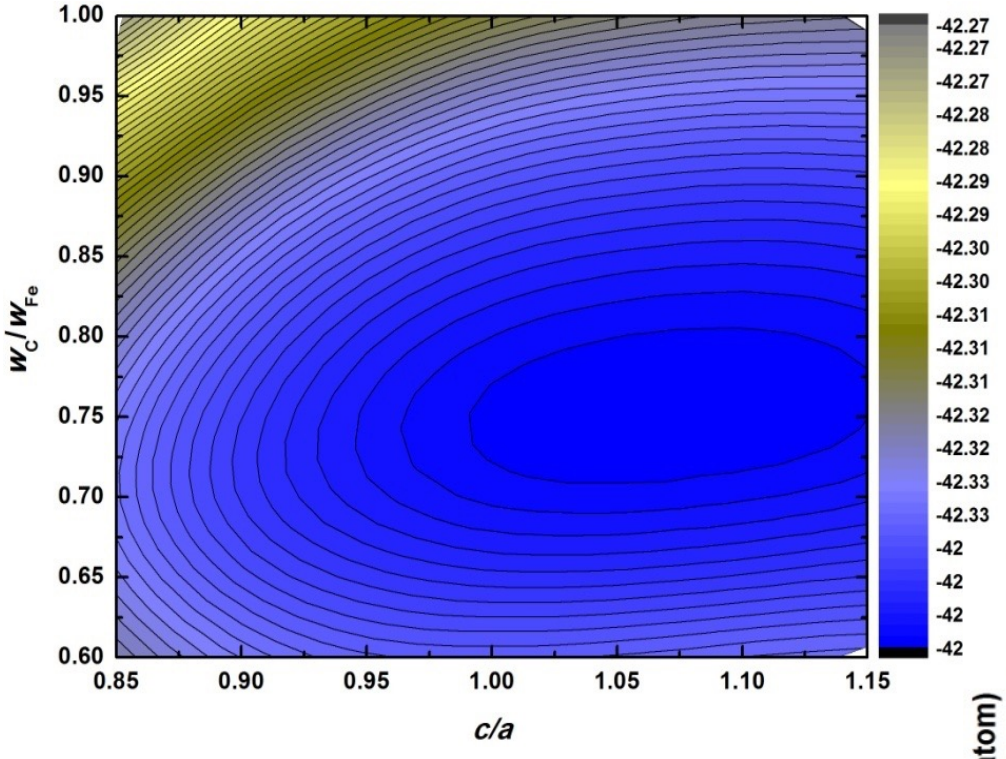

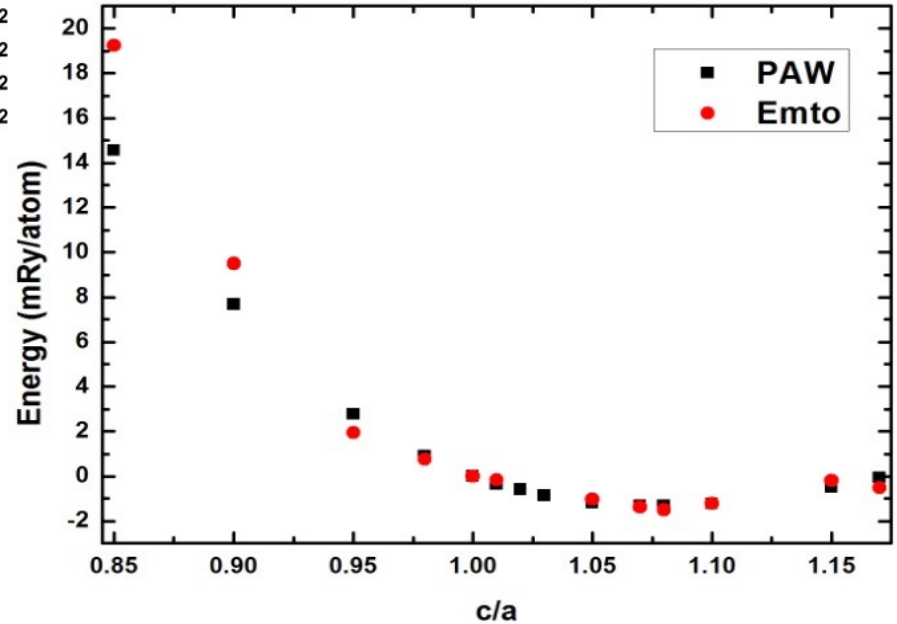

Coherent Potential Approximation

Soven, Győrffy
1960', 1970'

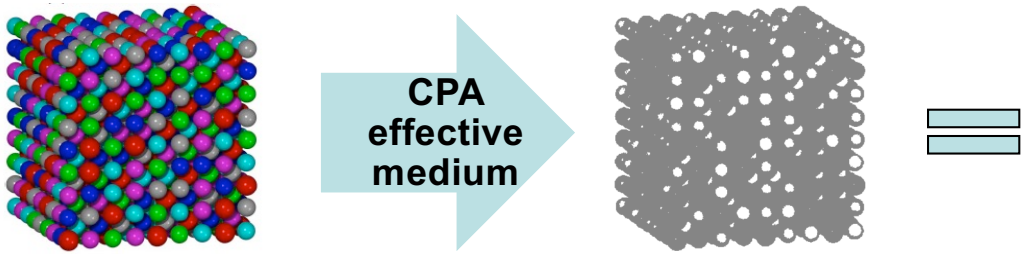

$A_1, A_2, A_3, A_4, A_5, \ldots, A_N$

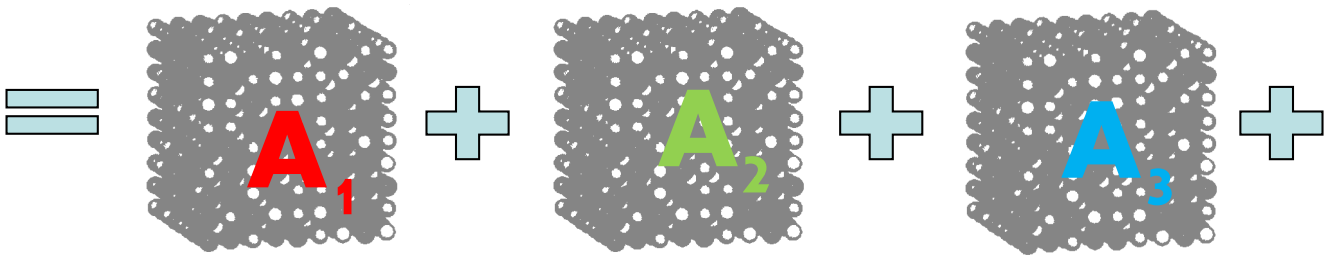

We solve N single impurity problems
(order-N in terms of alloy components)

The EMTO-CPA method for alloys

Kink cancelation for the effective medium

$$\sum_{Q''L''} a_{Q'} \left[S_{Q'L'Q''L''}(\kappa^2, \mathbf{k}) - \delta_{Q'Q''} \tilde{D}_{Q'L'Q'L''}(z) \right] \times \tilde{g}_{Q''L''QL}(z, \mathbf{k}) = \delta_{Q'Q} \delta_{L'L},$$

Impurity Green's function (Dyson eq.)

Effective medium Green's function

$$\tilde{g}_{QLQL'}(z) = \sum_i c_Q^i \, g^i_{QLQL'}(z),$$

$$g^i_{QLQL'}(z) = \tilde{g}_{QLQL'}(z) + \sum_{L''L'''} \tilde{g}_{QLQL''}(z) \times \left[D^i_{Ql''}(z) \delta_{L''L'''} - \tilde{D}_{QL''QL'''}(z) \right] g^i_{QL'''QL'}(z),$$

Self-consistent solution is needed.

Similar like in EMTO but now it includes the impurity potentials and Green's functions.

Total energy in EMTO/EMTO-CPA (The Full Charge Density method)

After we solve the KS equation

$$\{-\nabla^2 + v([n];r)\}\Psi_j(r) = \varepsilon_j \Psi_j(r)$$

we construct the total charge density

$$n(r) = \sum_{\varepsilon_j \leq \varepsilon_F} |\Psi_j(r)|^2$$

and then compute the total energy (valid both for ordered and disordered systems):

$$E[n] = T_s[n] + \frac{1}{2}\int v_H([n];r)n(r)dr + \int v_e([n];r)n(r)dr + E_{xc}[n]$$

c^i is the concentration for alloy component i

$$E_{tot} = T_s[n] + \sum_R \sum_i c^i \left(F^i_{intraR}[n^i_R] + E^i_{xcR}[n^i_R]\right) + F_{inter}[Q] + \Delta E^{SIM}.$$

The last term is a “small” correction for random alloys (if CPA is involved).

Annex: All integrations over the Wigner-Seitz cells are computed using the shape function technique

$$\sigma_R(\mathbf{r}_R) \equiv \begin{cases} 1 & \text{for } \mathbf{r}_R \in \Omega_R \\ 0 & \text{otherwise} \end{cases} .$$

$$\sigma_R(\mathbf{r}_R) = \sum_L \sigma_{RL}(r_R) Y_L(\hat{r}_R).$$

$$\int_{\Omega_R} n_R(\mathbf{r}_R)\, K([n];\mathbf{r}_R)\, d\mathbf{r}_R = \int_{s_R^c} \sigma_R(\mathbf{r}_R)\, n_R(\mathbf{r}_R)\, K([n];\mathbf{r}_R)\, d\mathbf{r}_R.$$

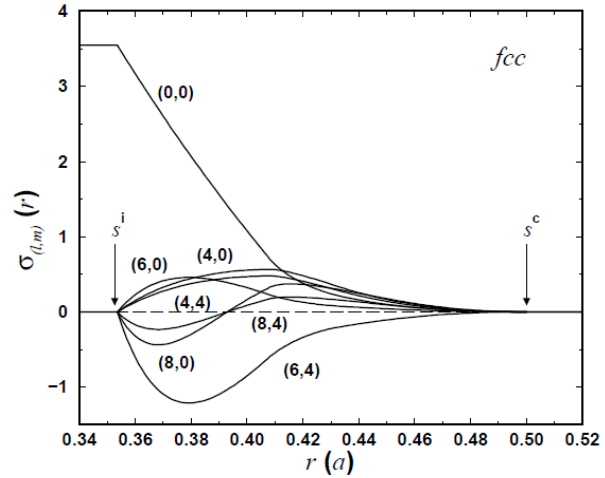

Ω is the WS cell,
s^c is the circumscribed sphere radius

$$\sigma_R(\mathbf{r}_R)\, n_R(\mathbf{r}_R) = \sum_L \tilde{n}_{RL}(r_R) Y_L(\hat{r}_R).$$

$$\boxed{\int_{\Omega_R} n_R(\mathbf{r}_R)\, K([n];\mathbf{r}_R)\, d\mathbf{r}_R = \sum_L \int_0^{s_R^c} \tilde{n}_{RL}(r_R) K_L(r_R) r_R^2 dr_R,}$$

$$K_L(r_R) \equiv \int K([n];\mathbf{r}_R) Y_L(\hat{r}_R) d\hat{r}_R$$

Most of the 3D integrals are reduced to 1D integrals.

Total energy: kinetic energy

Kinetic energy is computed from the Kohn-Sham wave functions or one-electron energies minus a potential dependent term:

$$T_s[n] \equiv \sum_{\epsilon_j \leq \epsilon_F} \int \Psi_j^*(\mathbf{r})(-\nabla^2)\Psi_j(\mathbf{r})d\mathbf{r}$$
$$= \sum_{\epsilon_j \leq \epsilon_F} \epsilon_j - \int n(\mathbf{r})v([n];\mathbf{r})d\mathbf{r}.$$

$$\mathrm{E[n]} = T_s[n] + \frac{1}{2}\int \mathrm{v_H([n];r)n(r)dr} + \int \mathrm{v_e([n];r)n(r)dr} + \mathrm{E_{xc}[n]}$$

The second equation comes from the Kohn-Sham equation.

The first term is the one electron energy or band energy.

Total energy: intracell energy

Intracell energy is the Coulomb energy between electrons within the unit cell:

$$E[n] = T_s[n] + \frac{1}{2}\int v_H([n];r)n(r)dr + \int v_e([n];r)n(r)dr + E_{xc}[n]$$

$$F^i_{intraR}[n^i_R] = \frac{\sqrt{4\pi}}{w}\sum_L \int_0^{s^c_R} \tilde{n}^i_{RL}(r_R)\left[\left(\frac{r_R}{w}\right)^l P^i_{RL}(r_R) + \left(\frac{r_R}{w}\right)^{-l-1} Q^i_{RL}(r_R) - 2Z^i_R\frac{w}{r_R}\delta_{L,L_0}\right] r_R^2 dr_R$$

$$P^i_{RL}(r_R) \equiv \frac{\sqrt{4\pi}}{2l+1}\int_{r_R}^{s^c_R} \tilde{n}^i_{RL}(r'_R)\left(\frac{r'_R}{w}\right)^{-l-1}(r'_R)^2 dr'_R,$$

$$Q^i_{RL}(r_R) \equiv \frac{\sqrt{4\pi}}{2l+1}\int_0^{r_R} \tilde{n}^i_{RL}(r'_R)\left(\frac{r'_R}{w}\right)^{l}(r'_R)^2 dr'_R.$$

Total energy: intercell energy

Intercell (Madelung) energy is the Coulomb energy between electrons within different unit cell:

$$F^{no}_{inter}[n] = \frac{1}{2w}\sum_{RR'}{}' \sum_{LL'} Q_{RL} M_{RLR'L'} Q_{R'L'}.$$

$$E[n] = T_s[n] + \frac{1}{2}\int v_H([n];r)n(r)dr + \int v_e([n];r)n(r)dr + E_{xc}[n]$$

Mutipole moment of the charge density:

$$Q^i_{RL} = \frac{\sqrt{4\pi}}{2l+1}\int_0^{s^c_R}\left(\frac{r_R}{w}\right)^l \tilde{n}^i_{RL}(r_R) r_R^2 dr_R - Z^i_R \delta_{L,L_0}.$$

$$Q_{RL} = \sum_i c^i_R Q^i_{RL},$$

$Q_{lm=0}$ moments for fcc (111) surface

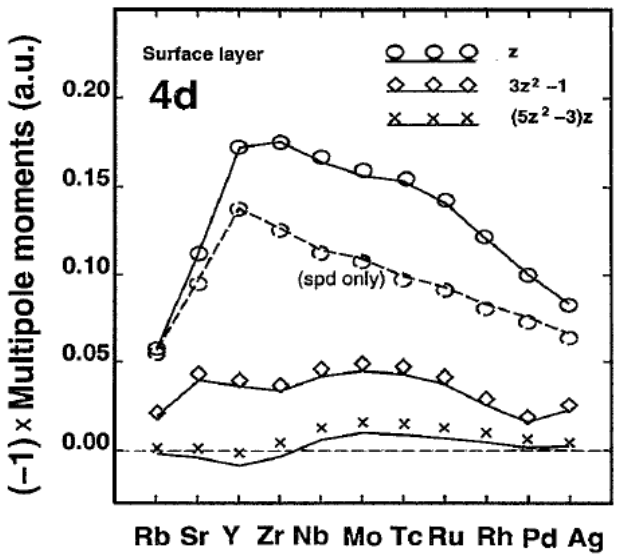

Total energy: xc energy

Exchange and correlation energy from 3D integration:

$$E[n] = T_s[n] + \frac{1}{2}\int v_H([n];r)n(r)dr + \int v_e([n];r)n(r)dr + E_{xc}[n]$$

$$E_{xc}[n_R] = \int_0^{2\pi}\int_0^{\pi}\int_0^{s_R^c} n_R^i(\mathbf{r}_R)\varepsilon_{xc}([n_R^i];\mathbf{r}_R) \times \sum_L^{l_{max}^s} \sigma_{RL}(r_R)Y_L(\hat{r}_R)\, r_R^2\, dr_R\, \sin\theta d\theta d\phi$$

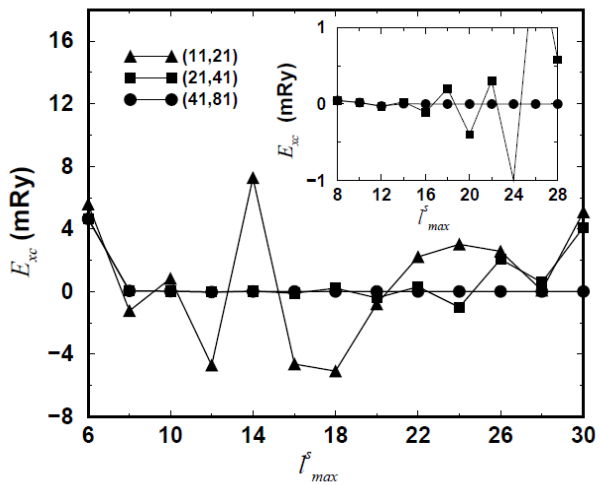

Very slow convergence with respect to the number of angular mesh points and *l*-truncation.

Demonstration

Pioneering test calculations

Bulk properties

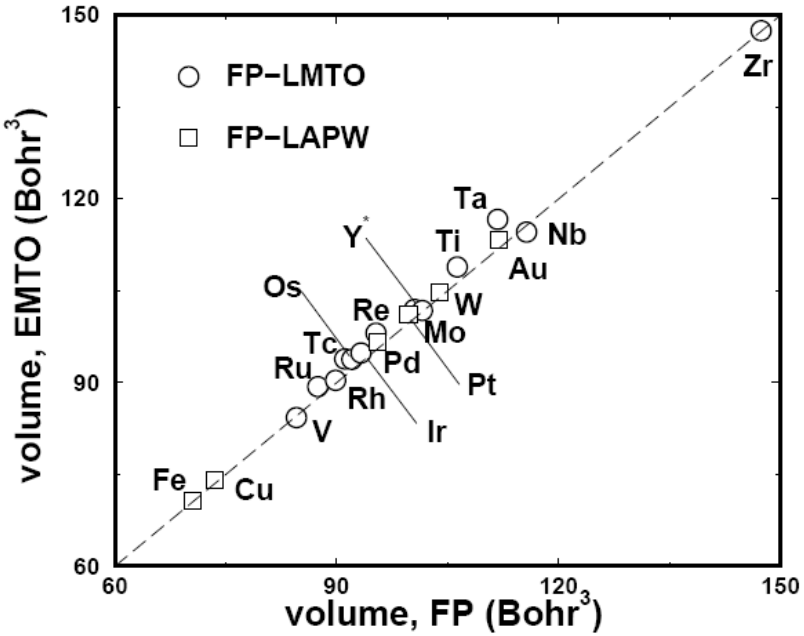

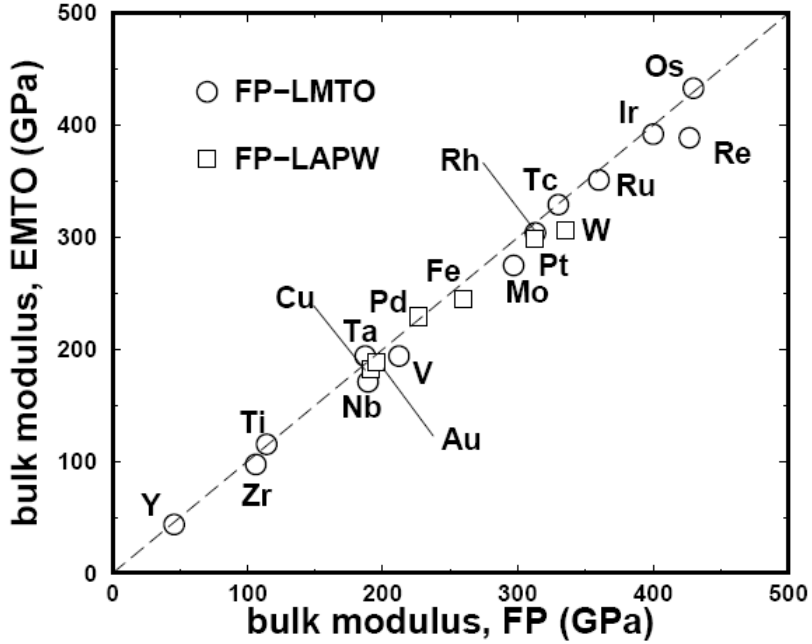

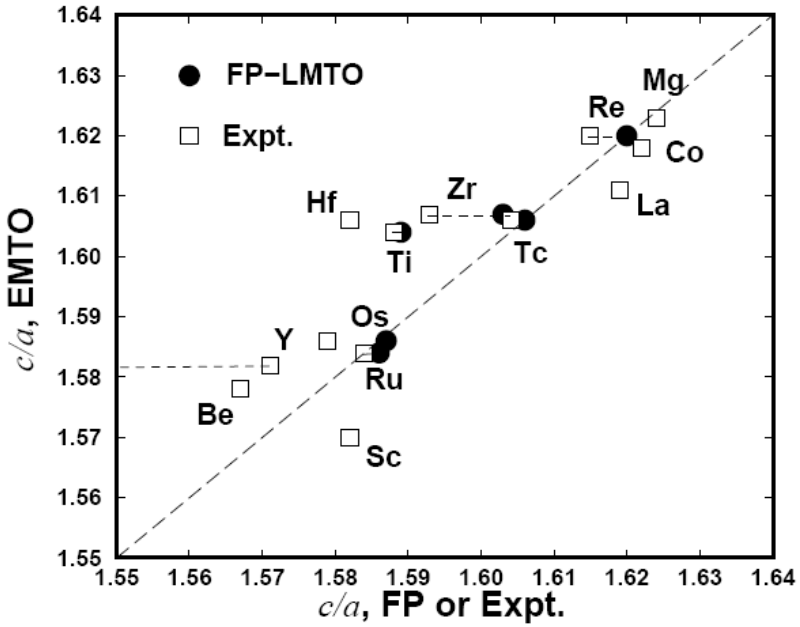

Surface properties: stress

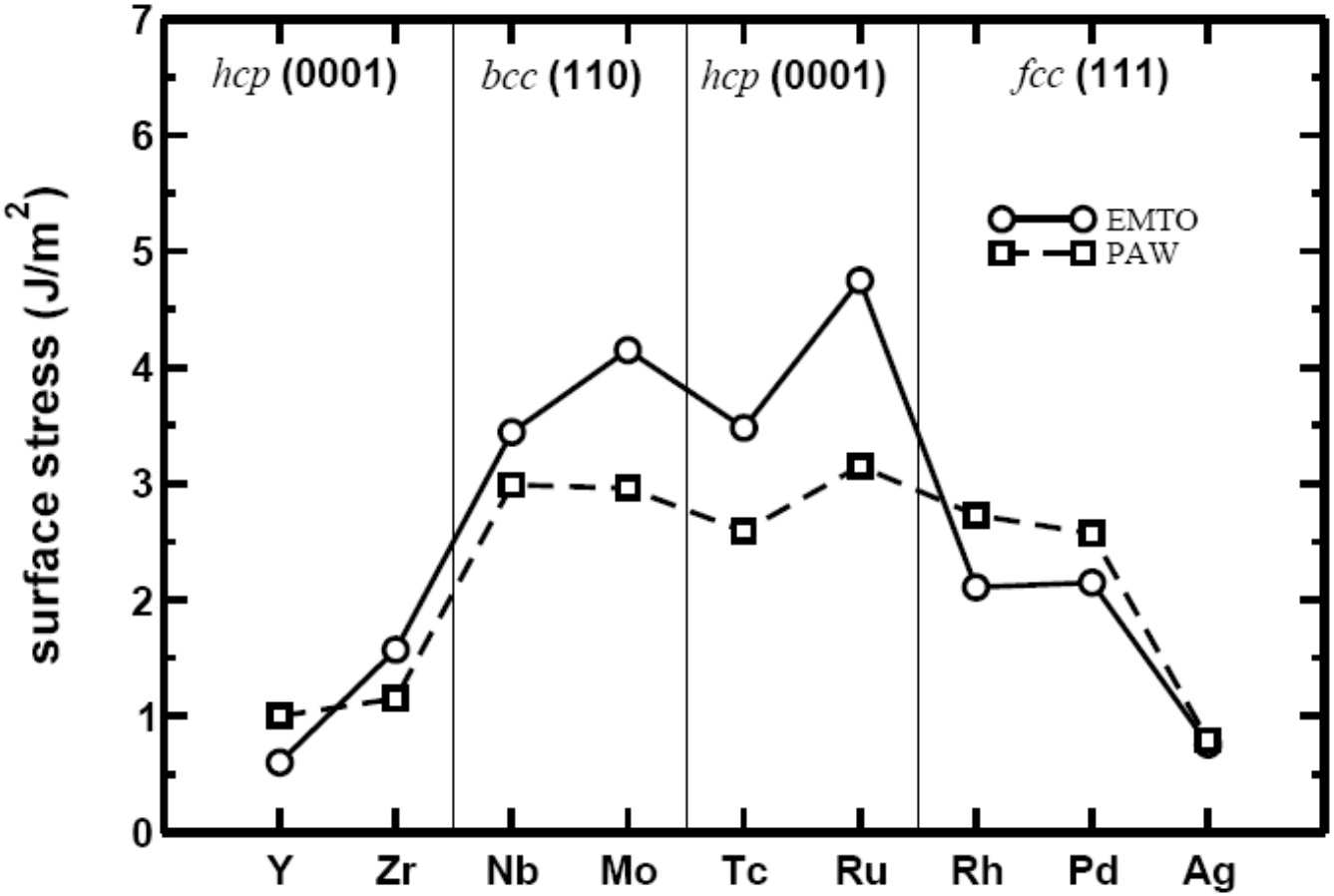

Fig. 7.7. Theoretical surface stress for the close-packed surfaces of 4*d* transition metal. Solid and dashed lines represent EMTO and PAW [168] results, respectively.

Demonstration

Alloys

Elastic properties

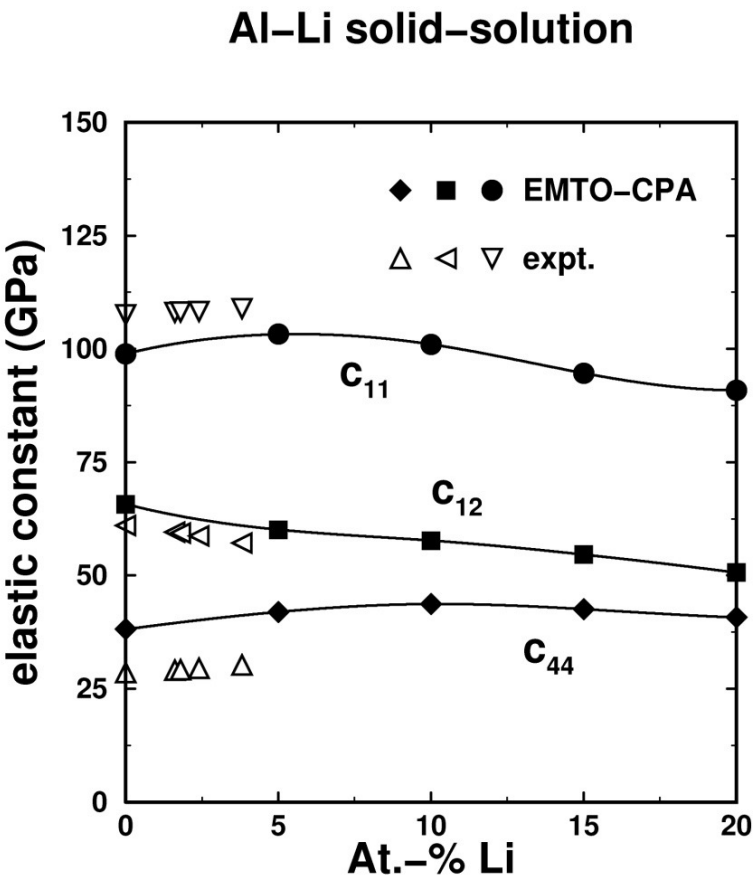

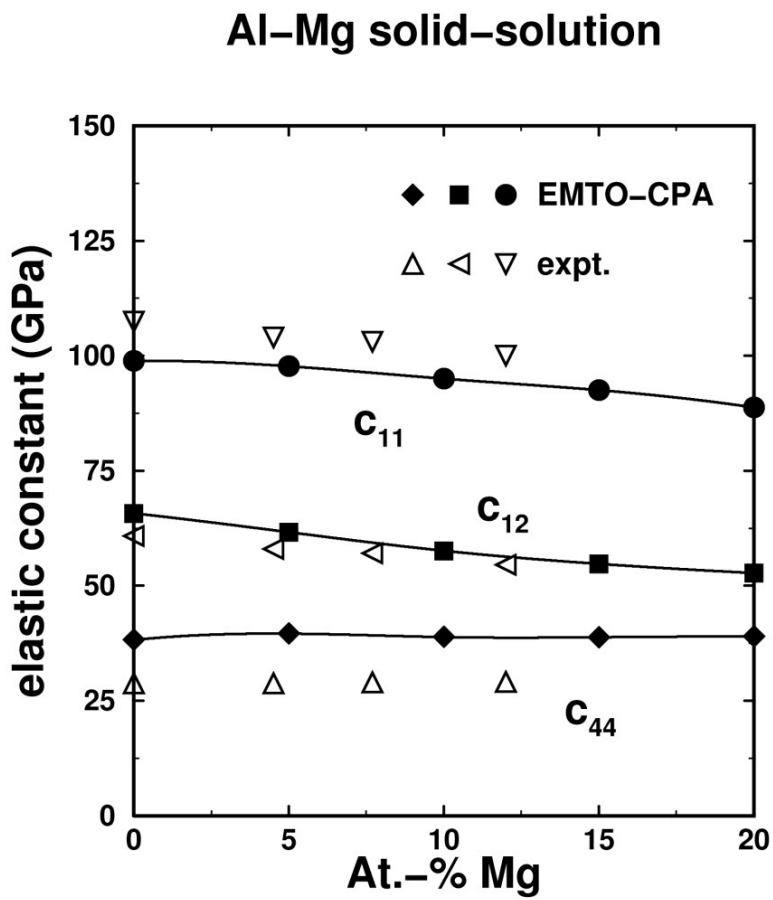

Elastic properties

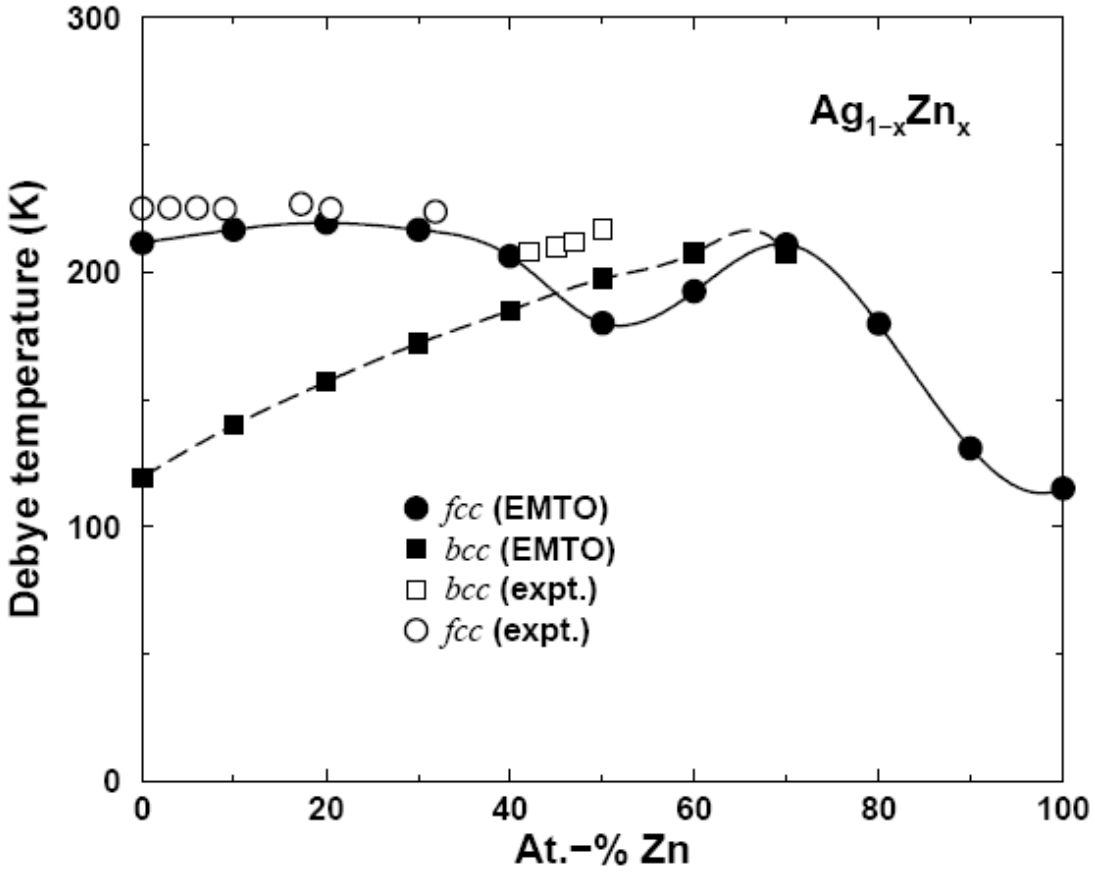

Fig. 8.18. The low temperature theoretical (EMTO-LDA) and experimental [239, 244] Debye temperatures of $Ag_{1-x}Zn_x$ random alloys in the *fcc* and *bcc* crystallographic phases [115].

Crystal structure, transformations

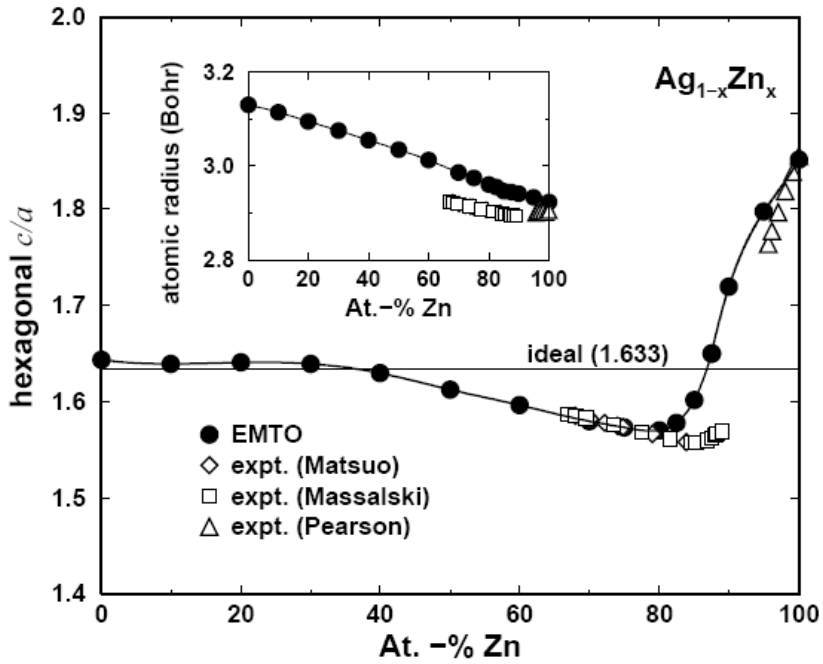

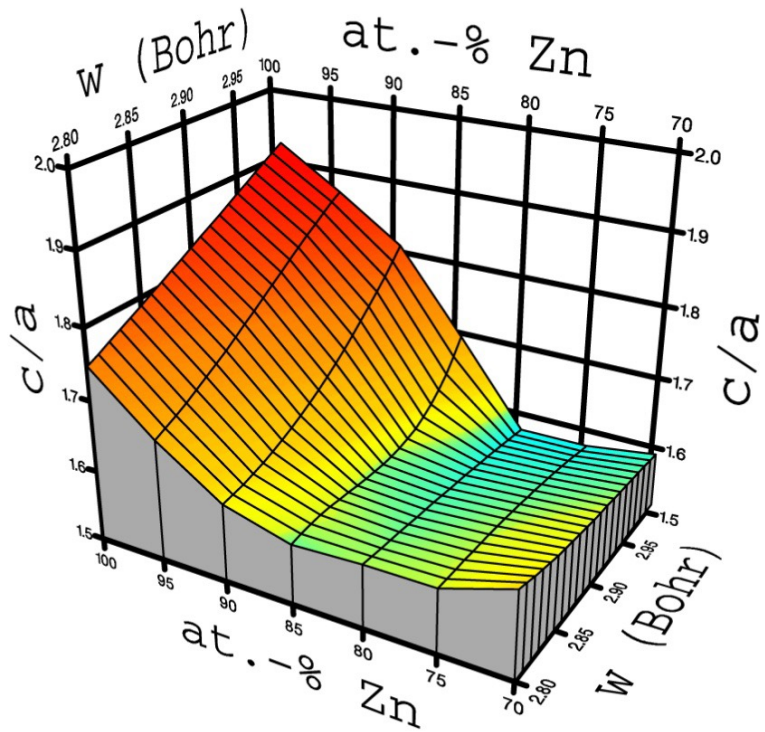

Fig. 8.19. Concentration dependence of the theoretical (EMTO-GGA) equilibrium axial ratio $(c/a)_0$ in *hcp* $Ag_{1-x}Zn_x$ alloys. The inset shows the calculated equilibrium atomic radii w as a function of Zn content. Experimental data are from Matsuo [248], Massalski [247] and Pearson [232].

Paramagnetic Fe

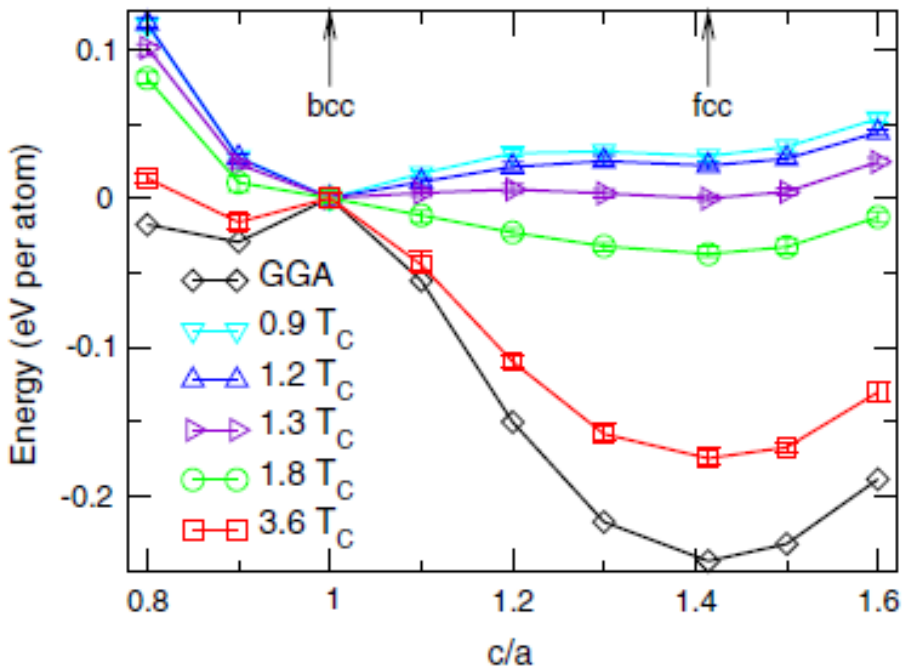

PRL 106, 106405 (2011) PHYSICAL REVIEW LETTERS week ending 11 MARCH 2011

Electronic Correlations at the α-γ Structural Phase Transition in Paramagnetic Iron

I. Leonov,[1] A. I. Poteryaev,[2,3] V. I. Anisimov,[2] and D. Vollhardt[1]
[1]*Theoretical Physics III, Center for Electronic Correlations and Magnetism, Institute of Physics, University of Augsburg, Augsburg 86135, Germany*
[2]*Institute of Metal Physics, Sofia Kovalevskaya Street 18, 620219 Yekaterinburg GSP-170, Russia*
[3]*Institute of Quantum Materials Science, 620107 Yekaterinburg, Russia*
(Received 25 August 2010; published 11 March 2011)

We compute the equilibrium crystal structure and phase stability of iron at the α(bcc) − γ(fcc) phase transition as a function of temperature, by employing a combination of *ab initio* methods for calculating electronic band structures and dynamical mean-field theory. The magnetic correlation energy is found to be an essential driving force behind the α-γ structural phase transition in paramagnetic iron.

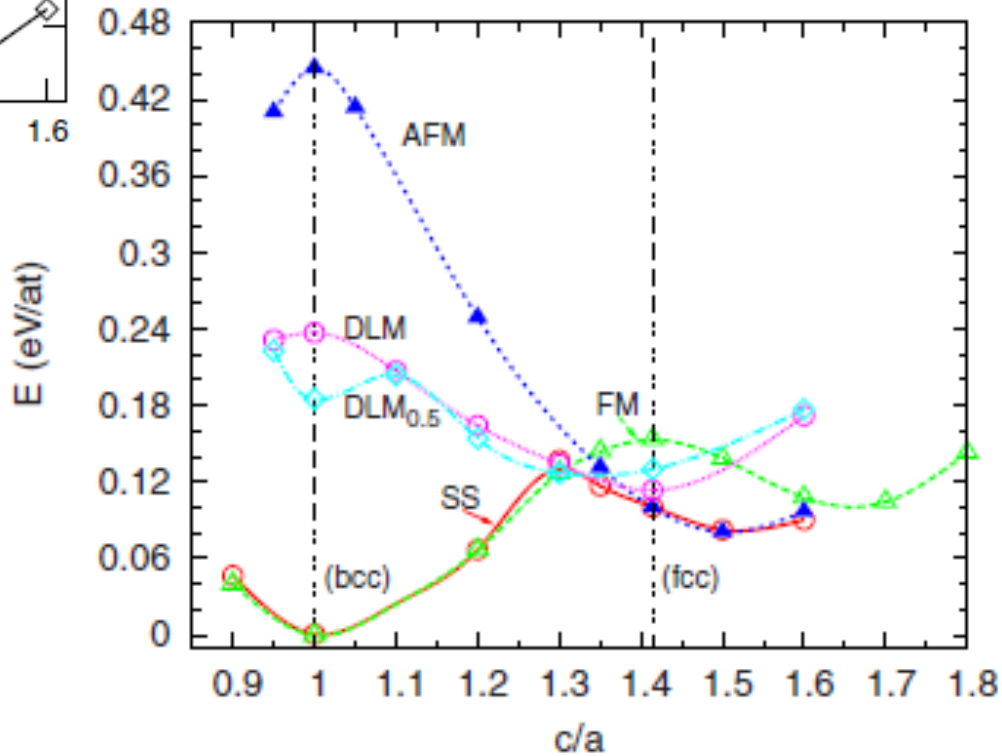

PHYSICAL REVIEW B 79, 094111 (2009)

Effect of magnetic state on the γ-α transition in iron: First-principles calculations of the Bain transformation path

S. V. Okatov
Institute of Quantum Materials Science, Ekaterinburg 620107, Russia

A. R. Kuznetsov and Yu. N. Gornostyrev
Ural Division, Institute of Metal Physics, Russian Academy of Sciences, Ekaterinburg 620041, Russia and Institute of Quantum Materials Science, Ekaterinburg 620107, Russia

V. N. Urtsev
Research and Technological Center "Ausferr," Magnitogorsk, 455023, Russia

M. I. Katsnelson
Institute for Molecules and Materials, Radboud University Nijmegen, NL-6525 AJ Nijmegen, The Netherlands
(Received 14 September 2008; revised manuscript received 23 February 2009; published 24 March 2009)

Paramagnetic Fe

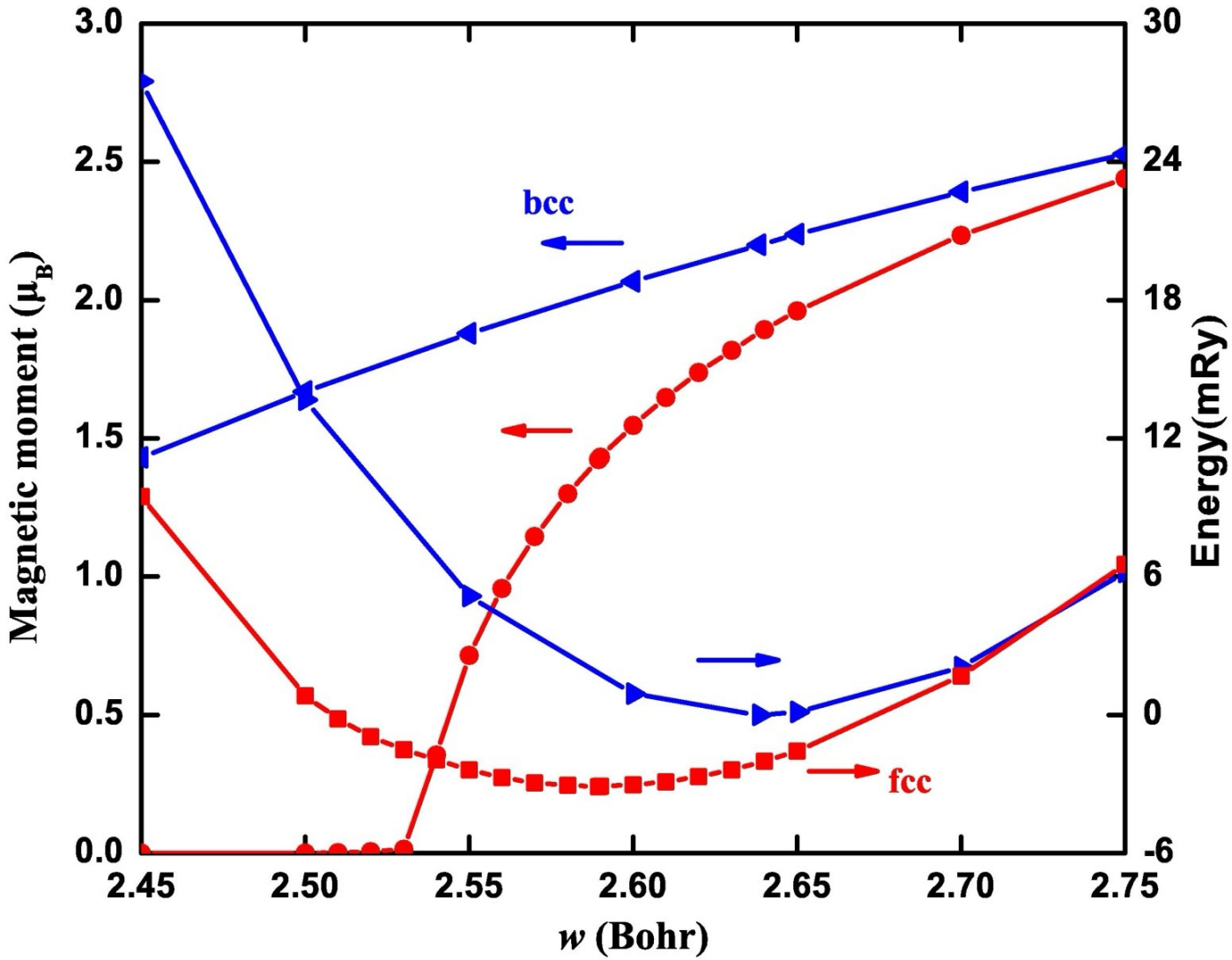

Paramagnetic Fe

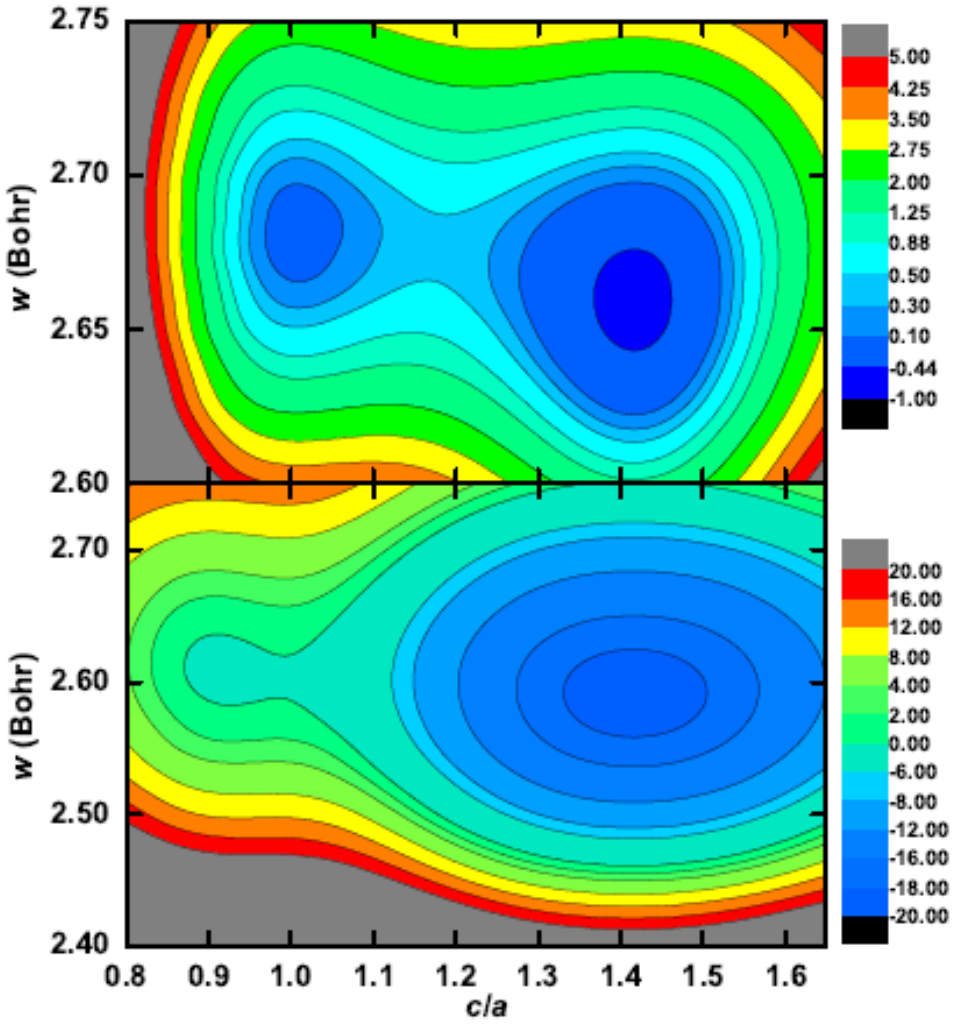

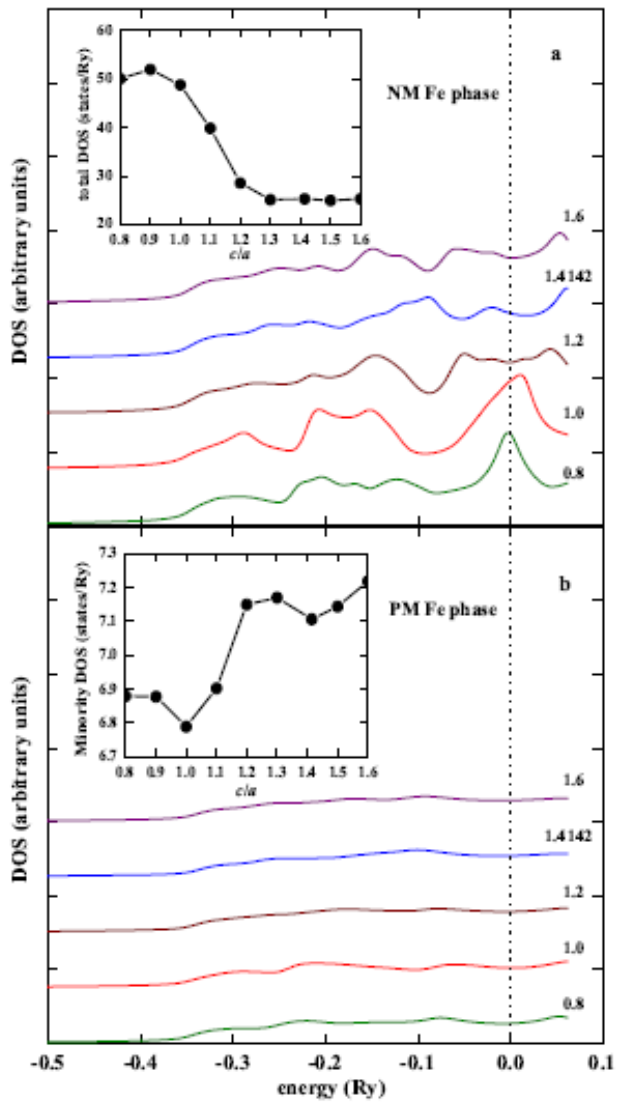

Paramagnetic FeCrNi alloys (stainless steel) Stacking-fault energy

Stainless steels

$Fe_{0.72}Cr_{0.2}Ni_{0.08}$

	V	c_{11}	c_{12}	c_{44}	A	B	G	B/G
EMTO	78.93	208.6	143.5	132.8	4.07	165.2	77.3	2.13
expt.	79.45	204.6	137.7	126.2	3.78	158.2	77.4	2.04
Δ	-0.6	2.0	4.2	5.2	7.6	4.4	-0.1	4.4

$$Fe^{\uparrow}_{(1-c-n)/2}Fe^{\downarrow}_{(1-c-n)/2}Cr^{\uparrow}_{c/2}Cr^{\downarrow}_{c/2}Ni^{\uparrow}_{n/2}Ni^{\downarrow}_{n/2}$$

- paramagnetic metals
- T_{mag}~50-100 K
- fcc structure

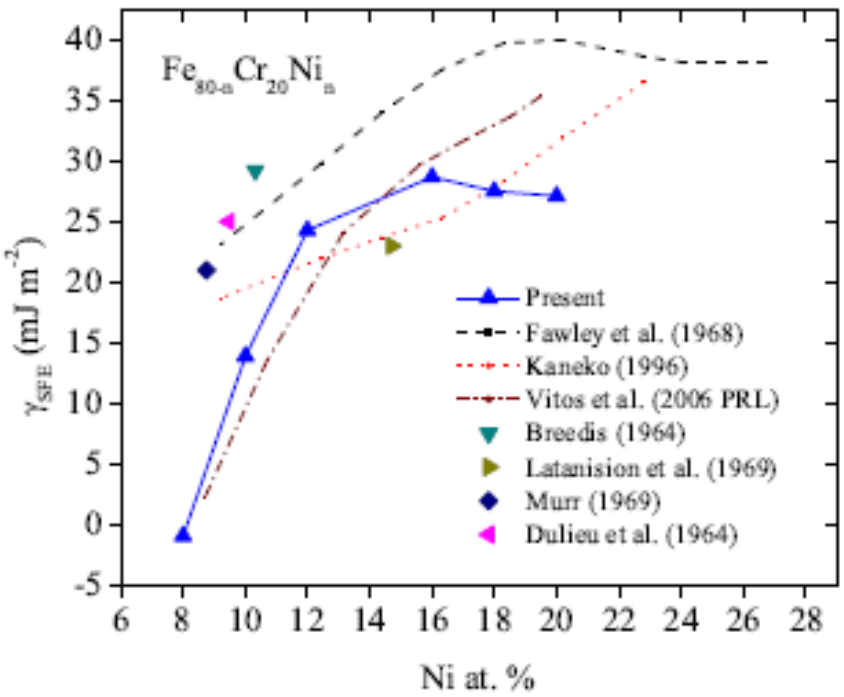

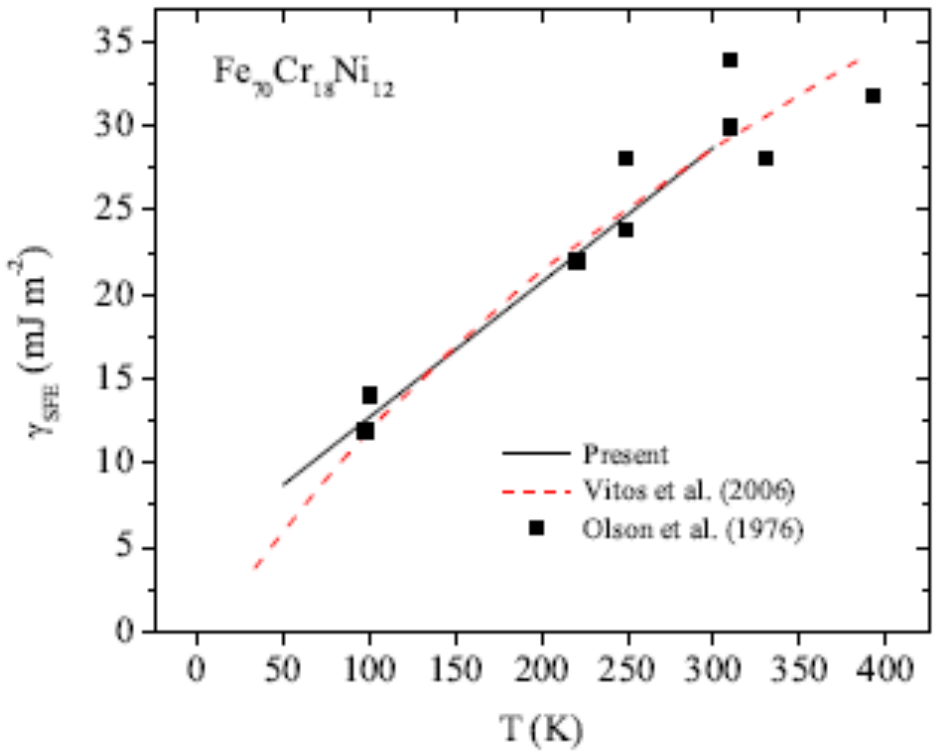

High Entropy Alloys

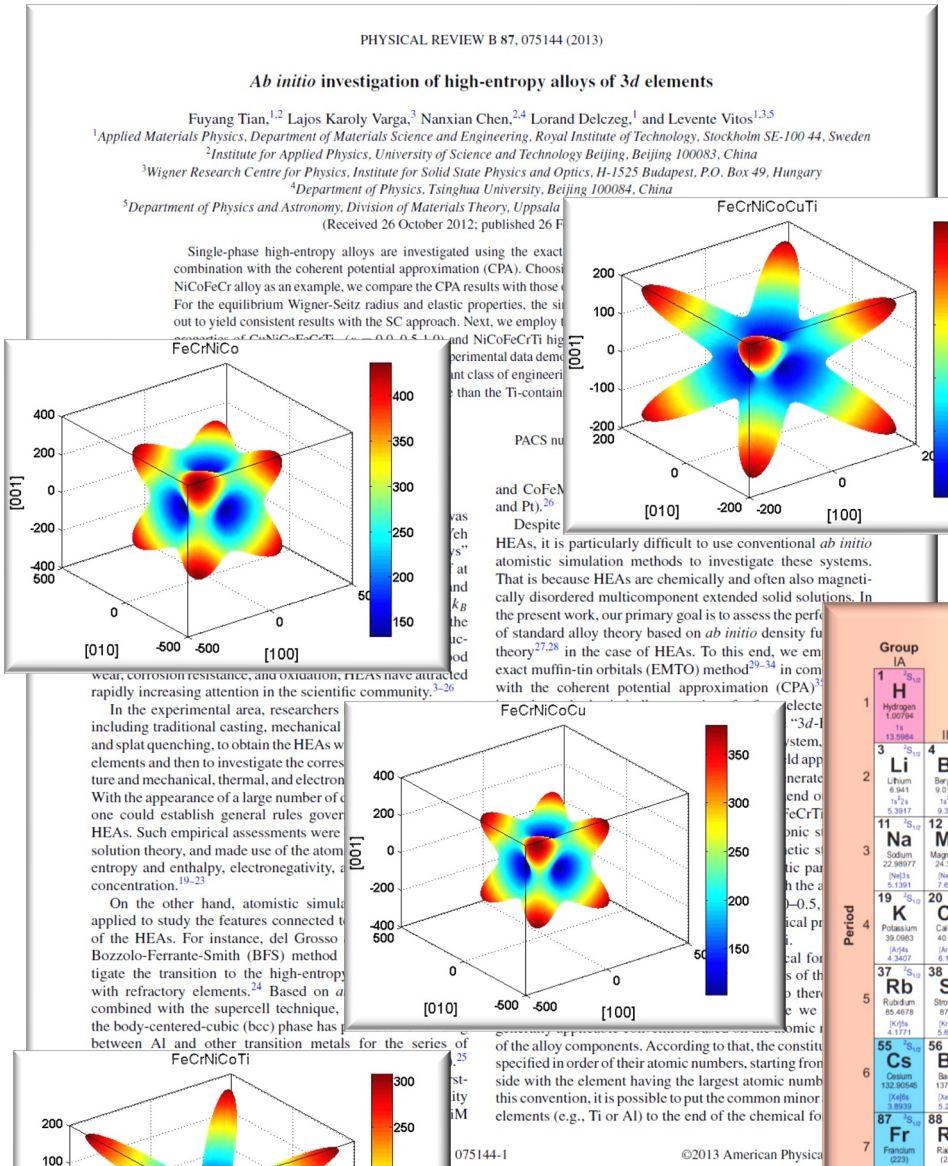

PHYSICAL REVIEW B 87, 075144 (2013)

Ab initio investigation of high-entropy alloys of 3*d* elements

Fuyang Tian,[1,2] Lajos Karoly Varga,[3] Nanxian Chen,[2,4] Lorand Delczeg,[1] and Levente Vitos[1,3,5]

[1]*Applied Materials Physics, Department of Materials Science and Engineering, Royal Institute of Technology, Stockholm SE-100 44, Sweden*
[2]*Institute for Applied Physics, University of Science and Technology Beijing, Beijing 100083, China*
[3]*Wigner Research Centre for Physics, Institute for Solid State Physics and Optics, H-1525 Budapest, P.O. Box 49, Hungary*
[4]*Department of Physics, Tsinghua University, Beijing 100084, China*
[5]*Department of Physics and Astronomy, Division of Materials Theory, Uppsala*
(Received 26 October 2012; published 26 F

Single-phase high-entropy alloys are investigated using the exact
combination with the coherent potential approximation (CPA). Choos
NiCoFeCr alloy as an example, we compare the CPA results with those
For the equilibrium Wigner-Seitz radius and elastic properties, the si
out to yield consistent results with the SC approach. Next, we employ t
and NiCoFeCrTi hig
perimental data dem
ant class of engineeri
than the Ti-contain

PACS nu

and CoFeN
and Pt).[26]
Despite
HEAs, it is particularly difficult to use conventional *ab initio*
atomistic simulation methods to investigate these systems.
That is because HEAs are chemically and often also magneti-
cally disordered multicomponent extended solid solutions. In
the present work, our primary goal is to assess the perf
of standard alloy theory based on *ab initio* density fu
theory[27,28] in the case of HEAs. To this end, we em
exact muffin-tin orbitals (EMTO) method[29–34] in com
with the coherent potential approximation (CPA)[3

wear, corrosion resistance, and oxidation, HEAs have attracted
rapidly increasing attention in the scientific community.[3–26]
In the experimental area, researchers
including traditional casting, mechanical
and splat quenching, to obtain the HEAs w
elements and then to investigate the corres
ture and mechanical, thermal, and electron
With the appearance of a large number of
one could establish general rules gover
HEAs. Such empirical assessments were
solution theory, and made use of the atom
entropy and enthalpy, electronegativity,
concentration.[19–23]
On the other hand, atomistic simula
applied to study the features connected t
of the HEAs. For instance, del Grosso
Bozzolo-Ferrante-Smith (BFS) method
tigate the transition to the high-entropy
with refractory elements.[24] Based on *a*
combined with the supercell technique,
the body-centered-cubic (bcc) phase has
between Al and other transition metals for the series of

of the alloy components. According to that, the constitu
specified in order of their atomic numbers, starting fron
side with the element having the largest atomic numb
this convention, it is possible to put the common minor
elements (e.g., Ti or Al) to the end of the chemical fo

075144-1 ©2013 American Physica

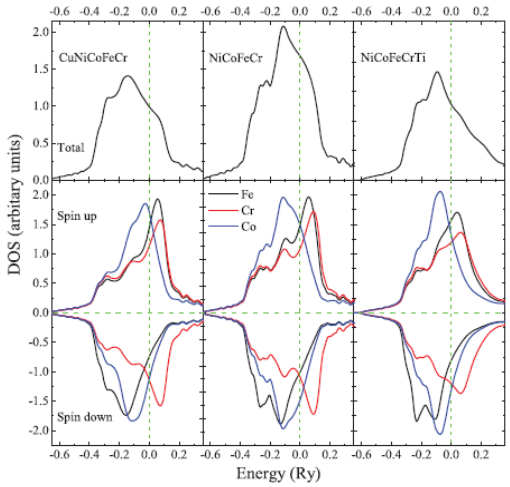

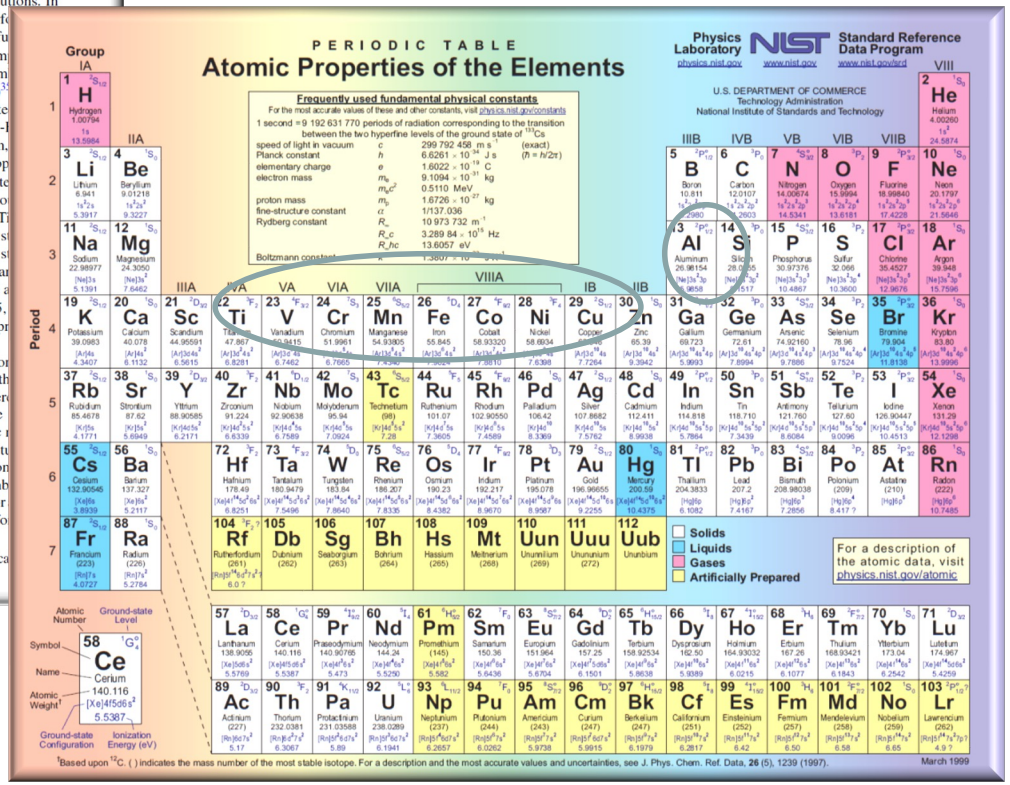

Phase stability of HEAs

PHYSICAL REVIEW B **00**, 005100 (2013)

Structural stability of NiCoFeCrAl$_x$ high-entropy alloy from *ab initio* theory

Fuyang Tian,[1,2] Lorand Delczeg,[1] Nanxian Chen,[2,3] Lajos Karoly Varga,[4] Jiang Shen,[2] and Levente Vitos[1,4,5]
[1]*Applied Materials Physics, Department of Materials Science and Engineering, Royal Institute of Technology, Stockholm SE-100 44, Sweden*
[2]*Institute for Applied Physics, University of Science and Technology Beijing, Beijing 100083, China*
[3]*Department of Physics, Tsinghua University, Beijing 100084, China*
[4]*Wigner Research Centre for Physics, Institute for Solid State Physics and Optics, H-1525 Budapest, P.O. Box 49, Hungary*
[5]*Department of Physics and Astronomy, Division of Materials Theory, Uppsala University, Box 516, SE-751210, Uppsala, Sweden*
(Received 2 April 2013; published xxxxx)

First-principles alloy theory predicts that at room temperature the paramagnetic NiCoFeCrAl$_x$ high entropy alloys adopt the face centered cubic (fcc) structure for $x \lesssim 0.60$ and the body centered cubic (bcc) structure for $x \gtrsim 1.23$, with an fcc-bcc duplex region in between the two pure phases. The calculated single- and polycrystal elastic parameters exhibit strong composition and crystal structure dependence. Based on the present theoretical findings, it is concluded that alloys around the equimolar NiCoFeCrAl composition have superior mechanical performance as compared to the single-phase regions.

DOI: 10.1103/PhysRevB.00.005100 PACS number(s): 62.20.D–, 71.20.Be, 81.05.Bx

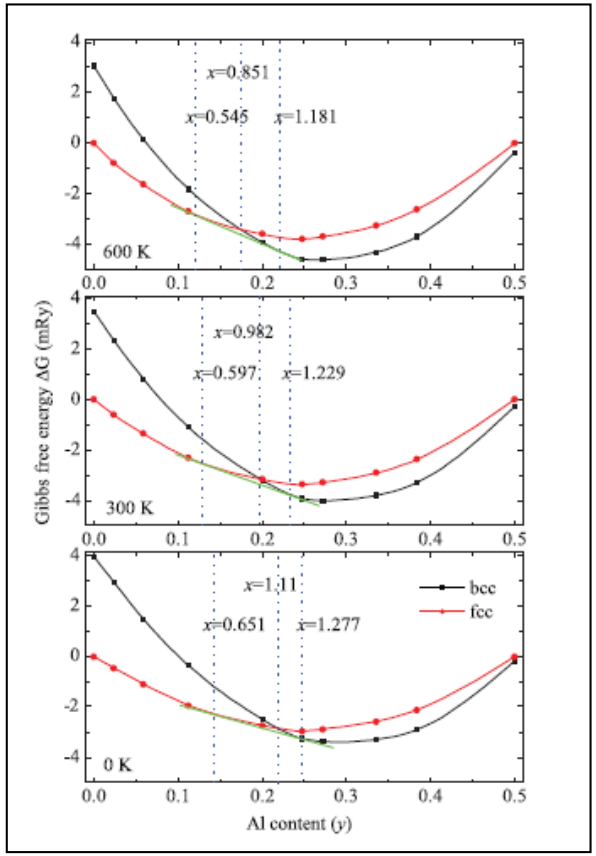

Theoretical and experimental phase boundaries in NiCoFeCrAlx-based HEAs

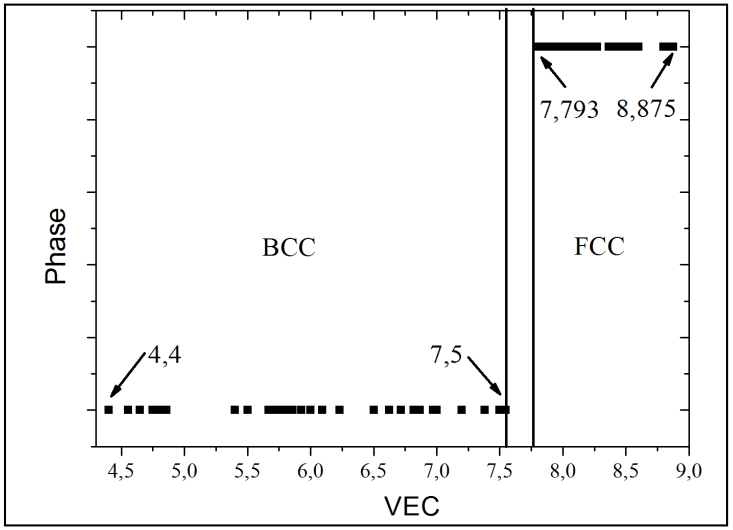

	$Al_xCrFeCoNi$		$Al_xCrMnFeCoNi$	
	fcc	bcc	fcc	bcc
x	0.651	1.277	0.488	1.658
c_{Al} (%)	13.4	24.2	8.9	24.9
VEC	7.52	6.98	7.56	6.75

Phase stability of HEAs

APPLIED PHYSICS LETTERS **107**, 251906 (2015)

Phase stability and magnetic behavior of FeCrCoNiGe high-entropy alloy

Shuo Huang,[1,a)] Ádám Vida,[2] Dávid Molnár,[2] Krisztina Kádas,[3,2] Lajos Károly Varga,[2,b)] Erik Holmström,[4] and Levente Vitos[1,2,3]

[1]*Applied Materials Physics, Department of Materials Science and Engineering, Royal Institute of Technology, Stockholm SE-100 44, Sweden*

[2]*Institute for Solid State Physics and Optics, Wigner Research Centre for Physics, P.O. Box 49, H-1525 Budapest, Hungary*

[3]*Department of Physics and Astronomy, Division of Materials Theory, Uppsala University, Box 516, SE-75120 Uppsala, Sweden*

[4]*Sandvik Coromant R&D, 126 80 Stockholm, Sweden*

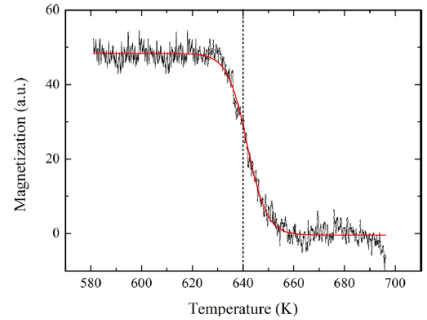

FIG. 3. Magnetization as a function of measured temperature for the as-cast FeCrCoNiGe alloy. The dashed line denotes the crossing point.

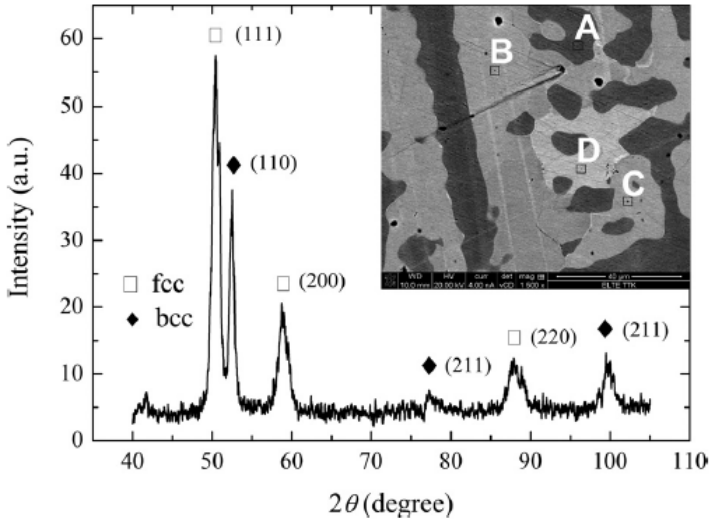

FIG. 1. XRD pattern of the as-cast FeCrCoNiGe alloy. The inset shows the SEM micrograph. The bright and dark fields are labeled by A, B, C, and D, which represent $Fe_{24.37}Cr_{21.71}Co_{22.97}Ni_{16.62}Ge_{14.33}$, $Fe_{18.07}Cr_{18.52}Co_{18.68}Ni_{22.27}Ge_{22.45}$, $Fe_{18.23}Cr_{18.61}Co_{18.79}Ni_{22.04}Ge_{22.33}$, and $Fe_{18.22}Cr_{18.48}Co_{18.73}Ni_{22.00}Ge_{22.57}$, respectively.

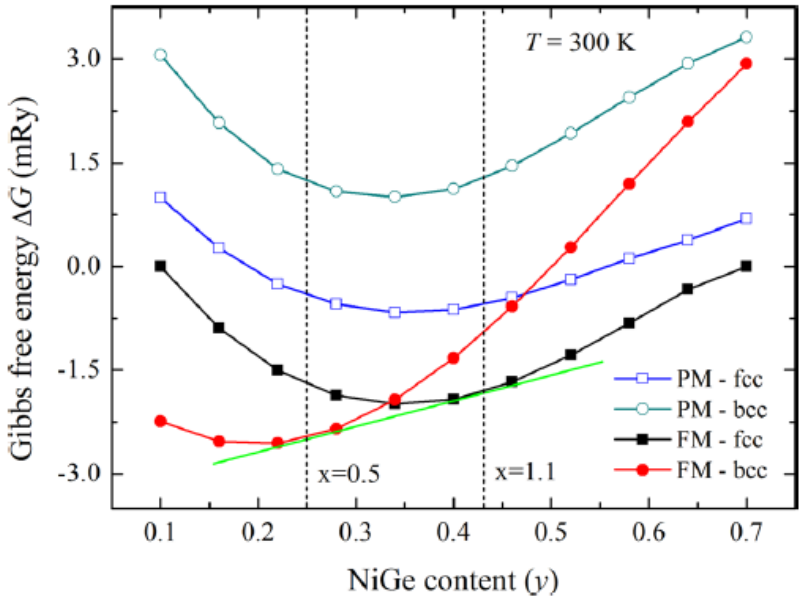

FIG. 2. Comparison of the Gibbs formation energies for fcc and bcc phases $(FeCrCo)_{1-y}(NiGe)_y$ $(0.1 \leq y \leq 0.7)$ in paramagnetic (PM) and ferromagnetic (FM) states as a function of NiGe content at room temperature. Note that $y = 2x/(3+2x)$, where x is the atomic fraction of NiGe in $FeCrCo(NiGe)_x$.

Elastic properties of HEAs

Contents lists available at ScienceDirec

Journal of Alloys and Compounds

journal homepage: www.elsevier.com/locate/jalcom

Ab initio design of elastically isotropic $TiZrNbMoV_x$ high-entropy alloys

Fuyang Tian [a,b,*], Lajos Karoly Varga [c], Nanxian Chen [b,d], Jiang Shen [b], Levente Vitos [a,c,e]

[a] Applied Materials Physics, Department of Materials Science and Engineering, Royal Institute of Technology, St
[b] Institute for Applied Physics, University of Science and Technology Beijing, Beijing 100083, China
[c] Institute for Solid State Physics and Optics, Wigner Research Centre for Physics, Hungarian Academy of Scienc
[d] Department of Physics, Tsinghua University, Beijing 100084, China
[e] Department of Physics and Astronomy, Division of Materials Theory, Uppsala University, Box 516, SE-751210

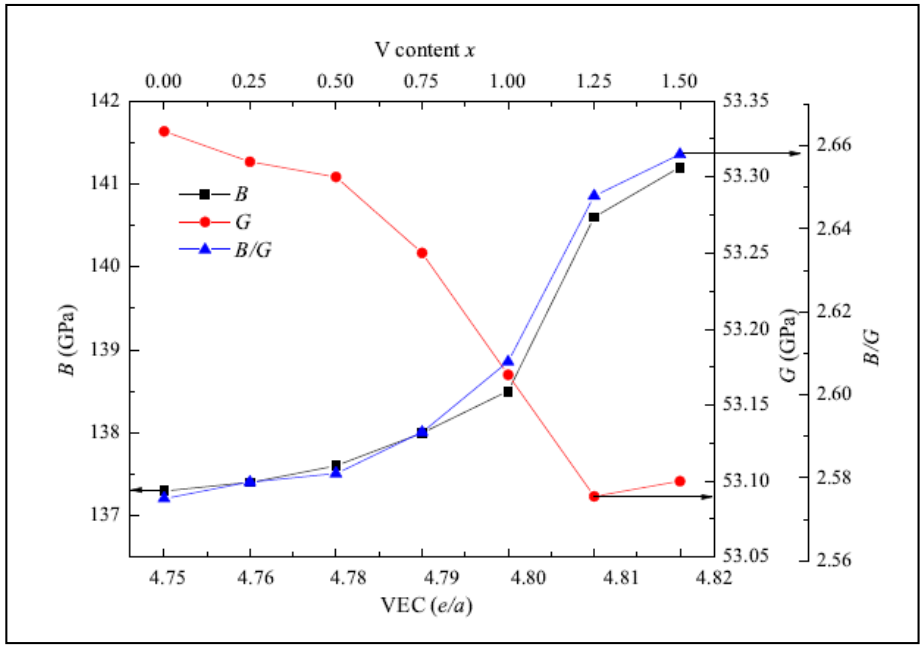

Theoretical prediction

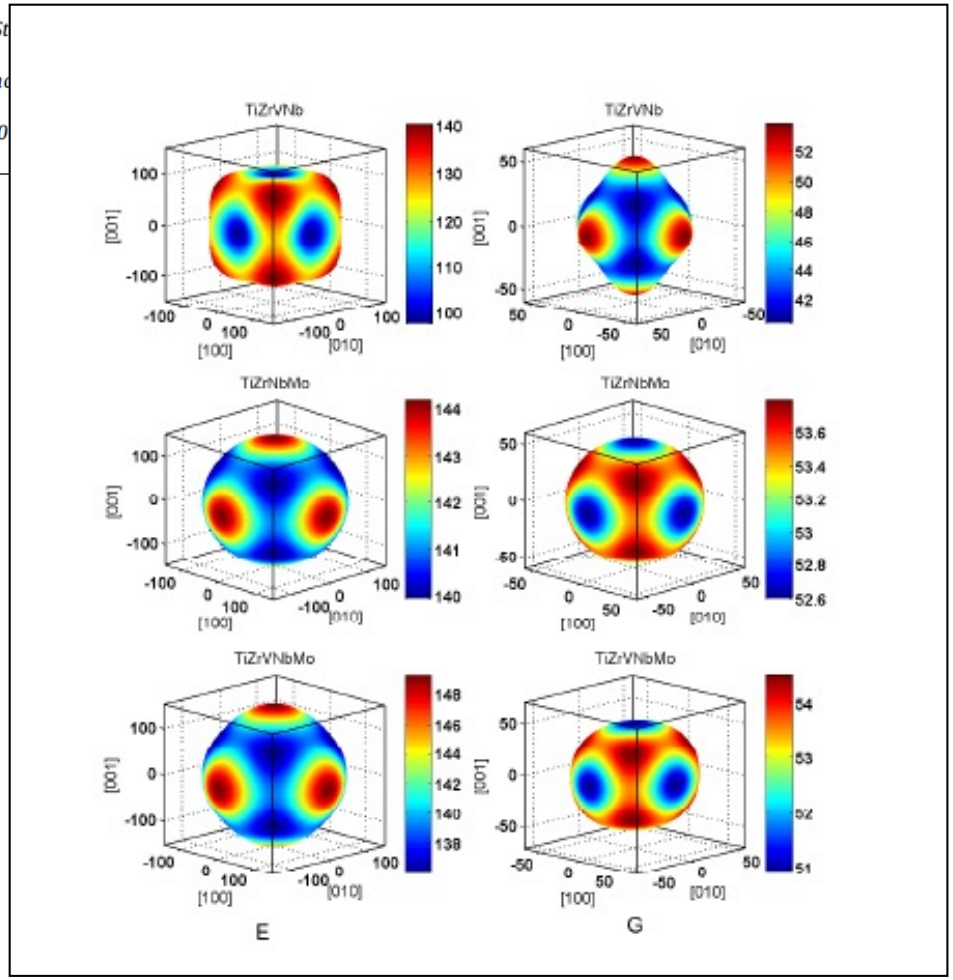

EMTO-CPA versus VASP-SQS

Materials and Design 114 (2017) 243–252

Contents lists available at ScienceDirect

Materials and Design

journal homepage: www.elsevier.com/locate/matdes

Alloying effect on the elastic properties of refractory high-entropy alloys

Li-Yun Tian[a,b], Guisheng Wang[c], Joshua S. Harris[d], Douglas L. Irving[d], Jijun Zhao[b], Levente Vitos[a,e,f]

[a]Applied Materials Physics, Department of Materials Science and Engineering, Royal Institute of Technology, Stockholm SE-100 44, Sweden
[b]Key Laboratory of Materials Modification by Laser, Ion, and Electron Beams of Ministry of Education, Dalian University of Technology, Dalian 116024, China
[c]School of Applied Mathematics and Physics, Beijing University of Technology, Beijing100124, China
[d]Department of Materials Science and Engineering, North Carolina State University, Raleigh, NC27695-7907, United States
[e]Department of Physics and Astronomy, Division of Materials Theory, Uppsala University, Box 516, SE-75121 Uppsala, Sweden
[f]Research Institute for Solid State Physics and Optics, Wigner Research Center for Physics, P.O. Box 49, Budapest H-1525, Hungary

LLD histograms VASP-SQS (bcc NN)

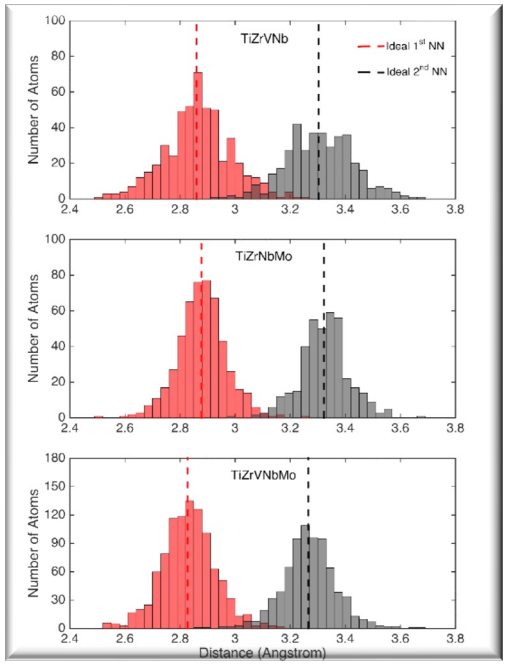

Elastic parameters

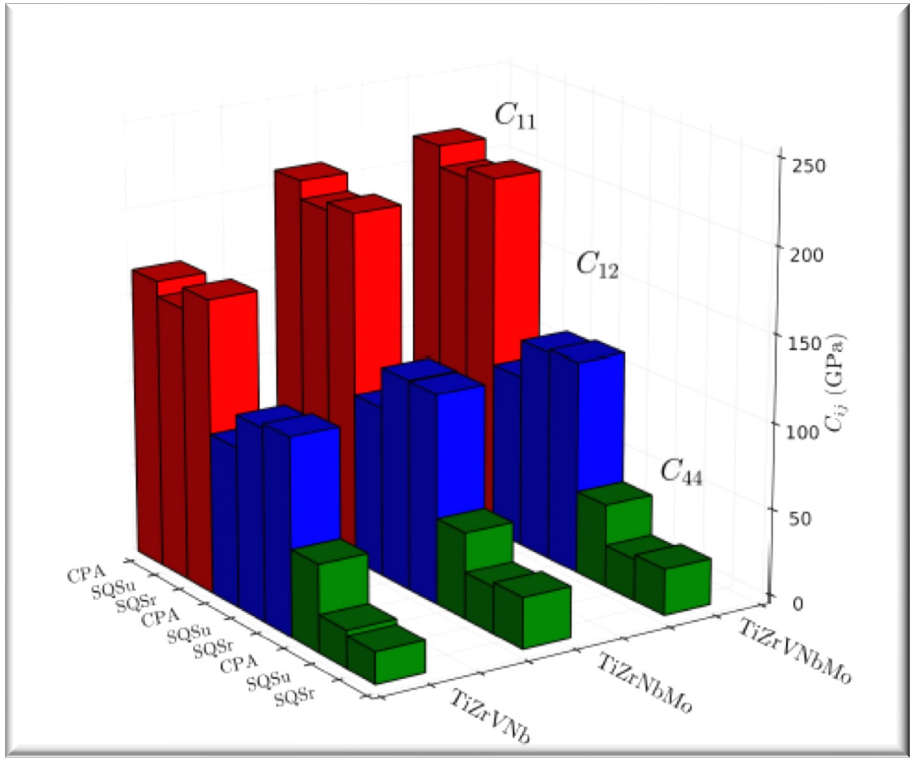

Mixing energy

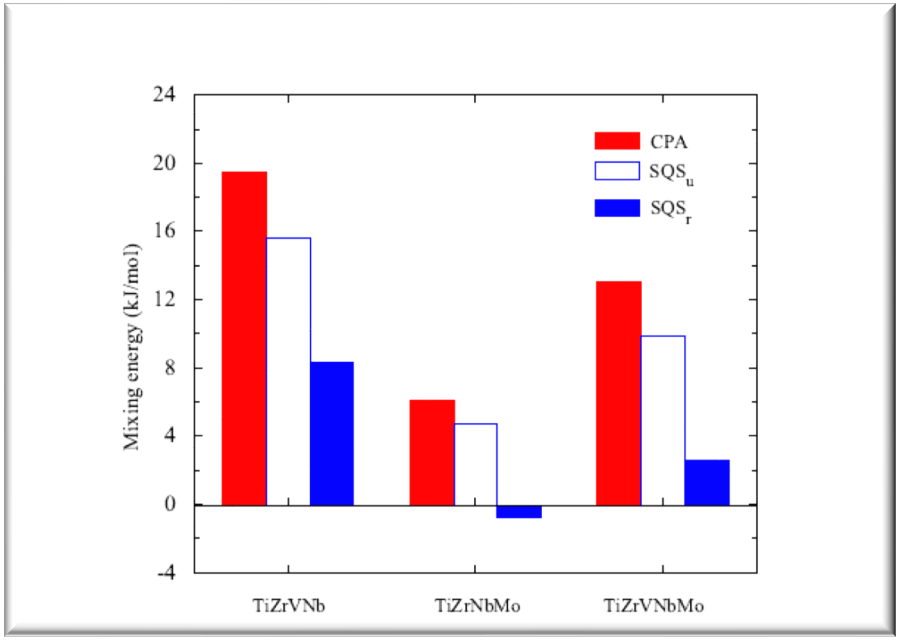

Magnetism in HEAs

Materials and Design 103 (2016) 71–74

Contents lists available at ScienceDirect

Materials and Design

journal homepage: www.elsevier.com/locate/matdes

Mechanism of magnetic transition in FeCrCoNi-based high entropy alloys

Shuo Huang [a,*], Wei Li [a], Xiaoqing Li [a], Stephan Schönecker [a], Lars Bergqvist [b], Erik Holmström [c], Lajos Károly Varga [d], Levente Vitos [a,d,e,**]

[a] Applied Materials Physics, Department of Materials Science and Engineering, Royal Institute of Technology, Stockholm SE-100 44, Sweden
[b] Department of Materials and Nano Physics, Royal Institute of Technology, Electrum 229, SE-16440 Kista, Sweden
[c] Sandvik Coromant R&D, 126 80, Stockholm, Sweden
[d] Institute for Solid State Physics and Optics, Wigner Research Centre for Physics, H-1525 Budapest, P.O. Box 49, Hungary
[e] Department of Physics and Astronomy, Division of Materials Theory, Uppsala University, Box 516, SE-75120 Uppsala, Sweden

Modeling based on Heisenberg Hamiltonian in combination with ab initio magnetic exchange parameters

$$H = -\sum_{i,j} J_{ij}\mathbf{m}_i\cdot\mathbf{m}_j,$$

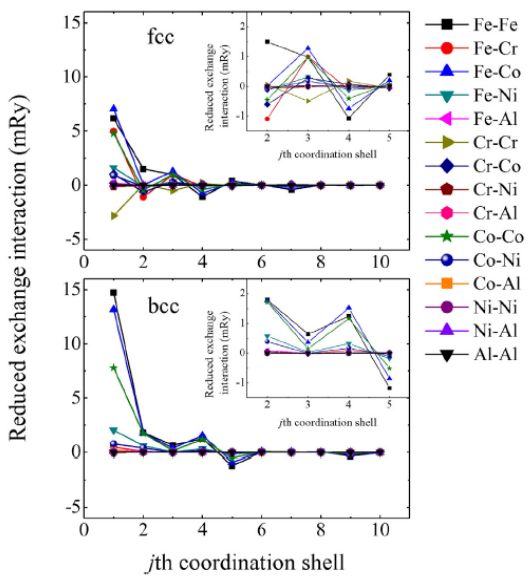

Fig. 2. Magnetic exchange interactions for equiatomic FeCrCoNiAl as a function of the coordination shell for fcc and bcc phases, respectively.

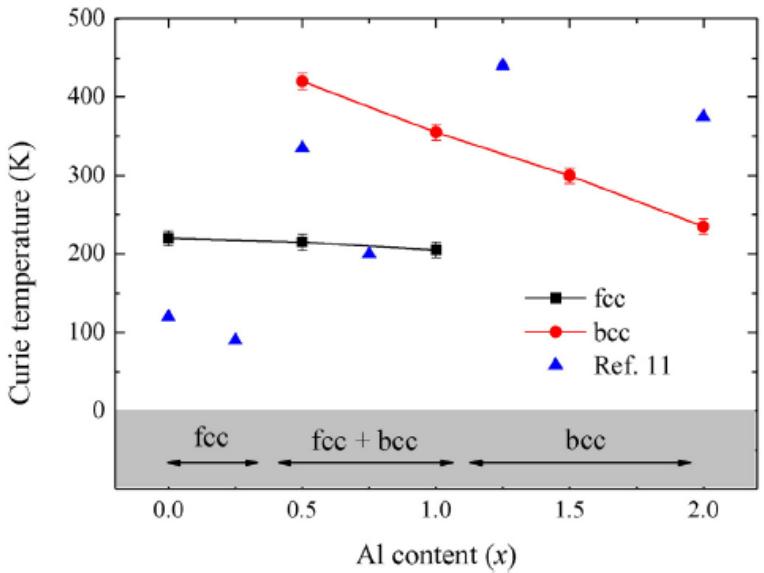

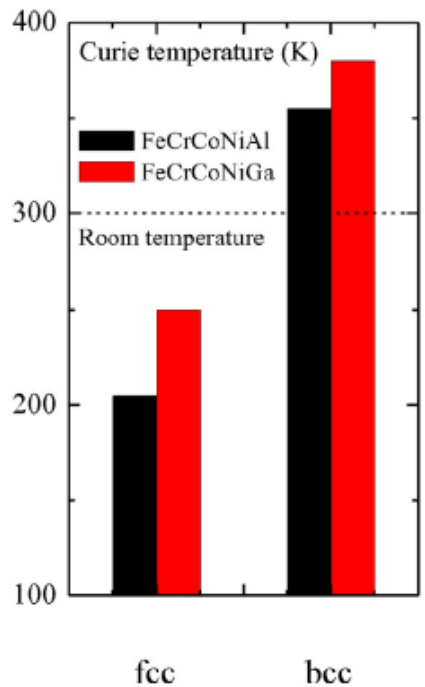

Magnetism in HEAs

Intermetallics 95 (2018) 80–84

Contents lists available at ScienceDirect

Intermetallics

journal homepage: www.elsevier.com/locate/intermet

Mapping the magnetic transition temperatures for medium- and high-entropy alloys

Shuo Huang[a,*], Erik Holmström[b], Olle Eriksson[c,d], Levente Vitos[a,c,e,**]

[a] Applied Materials Physics, Department of Materials Science and Engineering, Royal Institute of Technology, Stockholm, SE-100 44, Sweden
[b] Sandvik Coromant R&D, 126 80, Stockholm, Sweden
[c] Department of Physics and Astronomy, Division of Materials Theory, Uppsala University, Box 516, SE-75120, Uppsala, Sweden
[d] School of Science and Technology, Örebro University, SE-701 82, Örebro, Sweden
[e] Institute for Solid State Physics and Optics, Wigner Research Centre for Physics, P.O. Box 49, H-1525, Budapest, Hungary

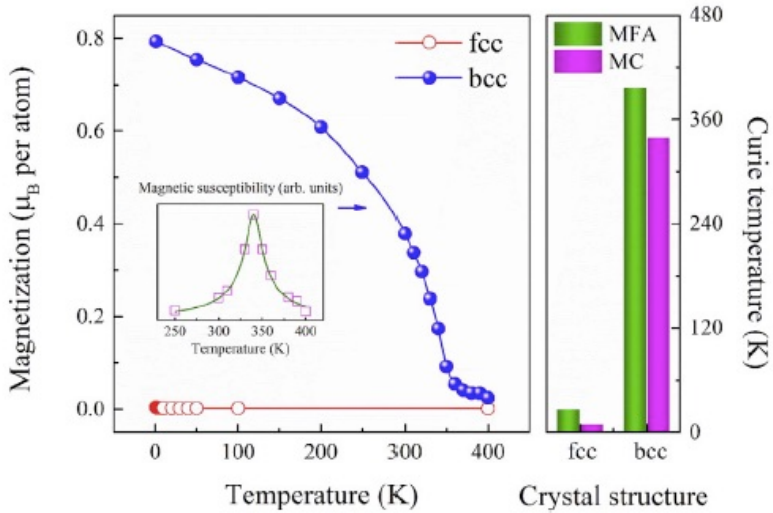

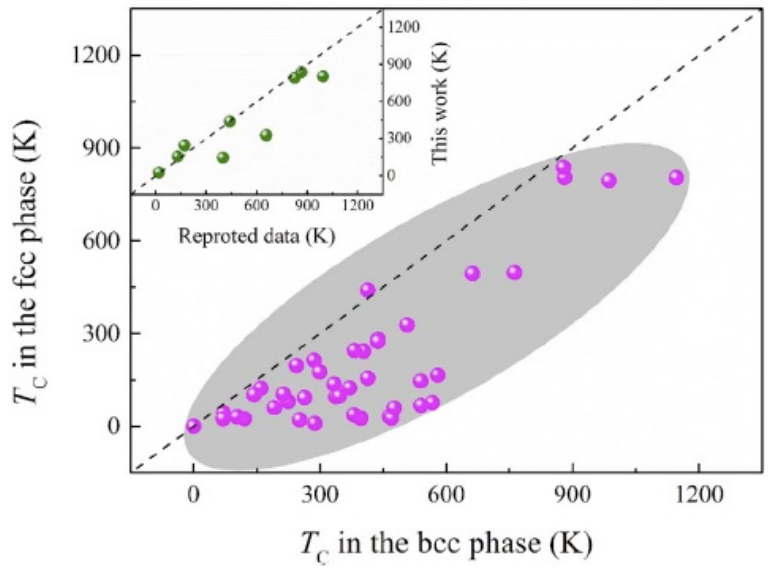

Longitudinal spin fluctuations in HEAs

SCIENTIFIC REPORTS

OPEN

Thermal spin fluctuations in CoCrFeMnNi high entropy alloy

Zhihua Dong[1], Stephan Schönecker[1], Wei Li[1], Dengfu Chen[2] & Levente Vitos[1,3,4]

Received: 21 May 2018
Accepted: 9 July 2018
Published online: 15 August 2018

High entropy alloys based on 3d transition metals display rich and promising magnetic characteristics for various high-technology applications. Understanding their behavior at finite temperature is, however, limited by the incomplete experimental data for single-phase alloys. Here we use first-principles alloy theory to investigate the magnetic structure of polymorphic CoCrFeMnNi in the paramagnetic state by accounting for the longitudinal spin fluctuations (LSFs) as a function of temperature. In both face-centered cubic (fcc) and hexagonal close-packed (hcp) structures, the LSFs induce sizable magnetic moments for Co, Cr and Ni. The impact of LSFs is demonstrated on the phase stability, stacking fault energy and the fcc-hcp interfacial energy. The hcp phase is energetically preferable to the fcc one at cryogenic temperatures, which results in negative stacking fault energy at these conditions. With increasing temperature, the stacking fault energy increases, suppressing the formation of stacking faults and nano-twins. Our predictions are consistent with recent experimental findings.

PHYSICAL REVIEW B **92**, 224420 (2015)

Thermal spin fluctuation effect on the elastic constants of paramagnetic Fe from first principles

Zhihua Dong,[1,2,*] Wei Li,[1] Stephan Schönecker,[1,*] Song Lu,[1] Dengfu Chen,[2,*] and Levente Vitos[1,3,4]
[1]*Applied Materials Physics, Department of Materials Science and Engineering, Royal Institute of Technology, Stockholm SE-100 44, Sweden*
[2]*College of Materials Science and Engineering, Chongqing University, Chongqing 400030, People's Republic of China*
[3]*Department of Physics and Astronomy, Division of Materials Theory, Uppsala University, Box 516, SE-75121 Uppsala, Sweden*
[4]*Research Institute for Solid State Physics and Optics, Wigner Research Center for Physics, P.O. Box 49, H-1525 Budapest, Hungary*
(Received 14 September 2015; published 15 December 2015)

PHYSICAL REVIEW B **96**, 174415 (2017)

Elastic properties of paramagnetic austenitic steel at finite temperature: Longitudinal spin fluctuations in multicomponent alloys

Zhihua Dong,[1,*] Stephan Schönecker,[1,†] Dengfu Chen,[2] Wei Li,[1] Mujun Long,[2] and Levente Vitos[1,3,4]
[1]*Applied Materials Physics, Department of Materials Science and Engineering, KTH - Royal Institute of Technology, SE-10044 Stockholm, Sweden*
[2]*College of Materials Science and Engineering, Chongqing University, Chongqing 400030, People's Republic of China*
[3]*Department of Physics and Astronomy, Division of Materials Theory, Uppsala University, Box 516, SE-75120 Uppsala, Sweden*
[4]*Research Institute for Solid State Physics and Optics, Wigner Research Center for Physics, P.O. Box 49, H-1525 Budapest, Hungary*
(Received 23 June 2017; revised manuscript received 30 October 2017; published 13 November 2017)

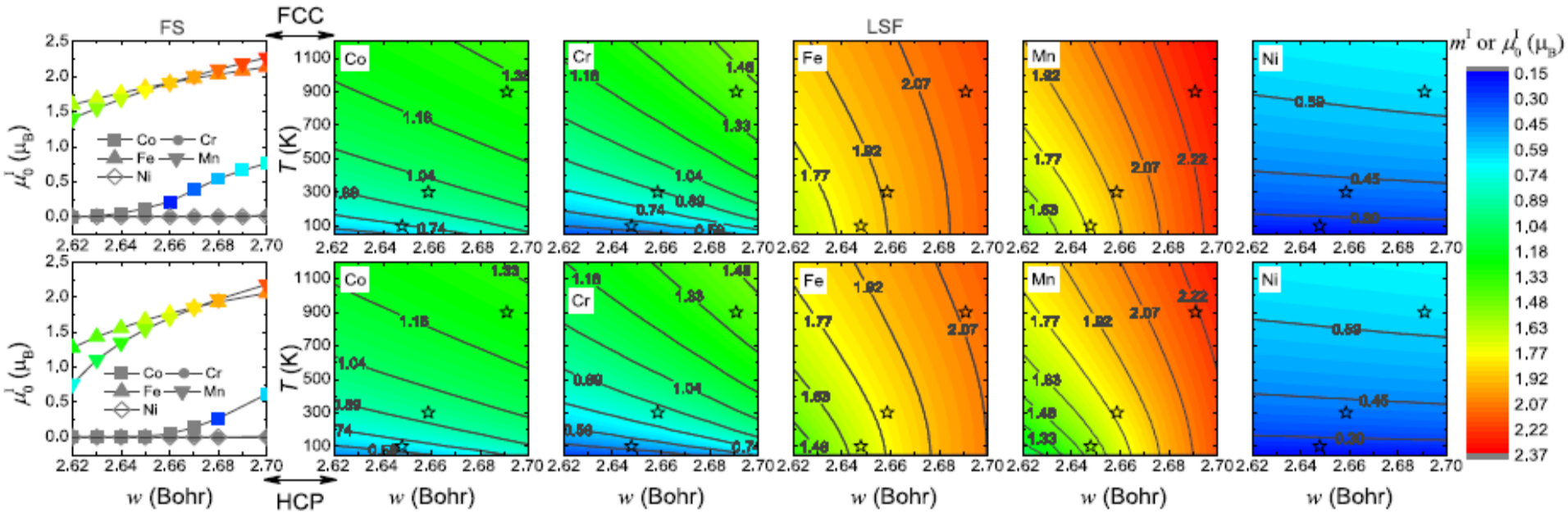

Thermal properties of HEAs

APPLIED PHYSICS LETTERS **110**, 241902 (2017)

Thermal expansion in FeCrCoNiGa high-entropy alloy from theory and experiment

Shuo Huang,[1,a)] Ádám Vida,[2,3,b)] Wei Li,[1] Dávid Molnár,[1,4] Se Kyun Kwon,[5] Erik Holmström,[6] Béla Varga,[7] Lajos Károly Varga,[2] and Levente Vitos[1,2,8,c)]

[1]*Applied Materials Physics, Department of Materials Science and Engineering, Royal Institute of Technology, Stockholm SE-100 44, Sweden*
[2]*Institute for Solid State Physics and Optics, Wigner Research Centre for Physics, P.O. Box 49, H-1525 Budapest, Hungary*
[3]*Department of Materials Physics, Eötvös University, Pázmány Péter Sétány 1/A, H-1117 Budapest, Hungary*
[4]*Materials Science Group, Dalarna University, 791 88 Falun, Sweden*
[5]*Graduate Institute of Ferrous Technology, Pohang University of Science and Technology, Pohang 37673, South Korea*
[6]*Sandvik Coromant R&D, 126 80 Stockholm, Sweden*
[7]*Faculty of Materials Science, Transylvania University of Brasov, Bulevardul Eroilor, No. 29, 500036 Brasov, Romania*
[8]*Department of Physics and Astronomy, Division of Materials Theory, Uppsala University, Box 516, SE-75120 Uppsala, Sweden*

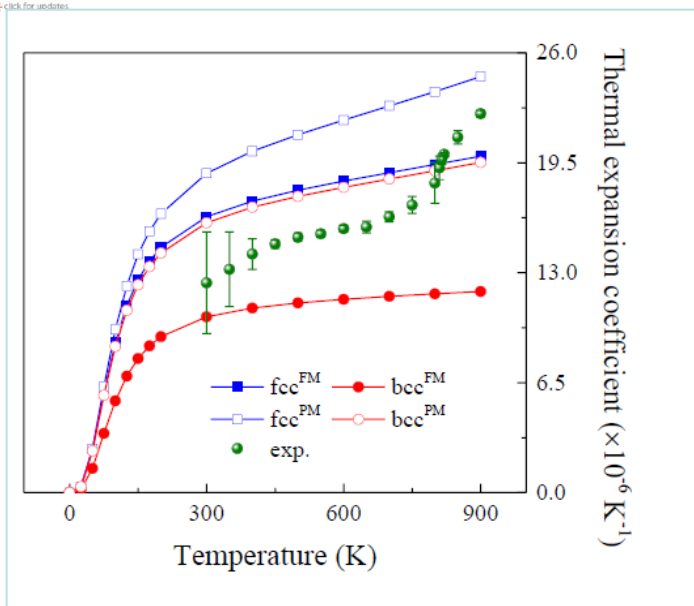

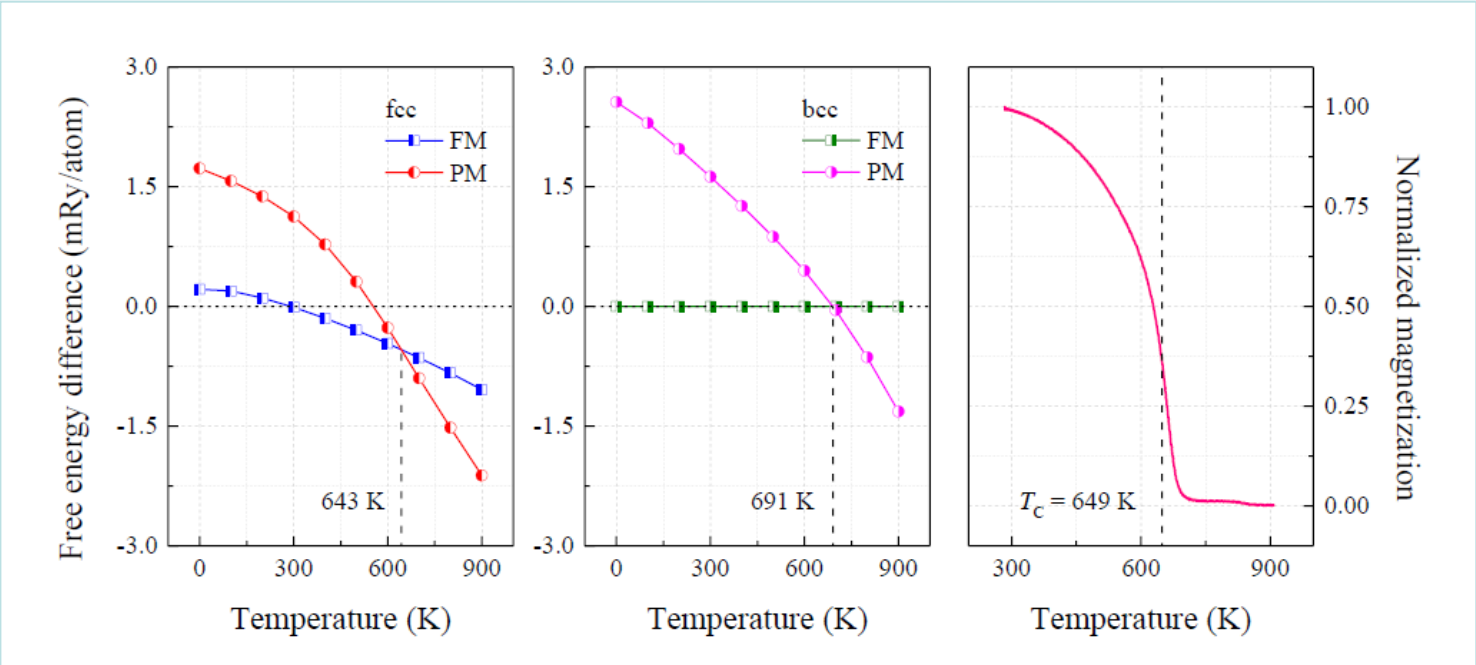

PHYSICAL REVIEW APP

HEA phase stability, precipitates

Strengthening Induced by MagnetoChemical Transition in Al-Doped Fe-Cr-Co-Ni High-Entropy Alloys

Shuo Huang,[1,*] Wei Li,[1] Erik Holmström,[2] and Levente Vitos[1,3,4]

[1] *Applied Materials Physics, Department of Materials Science and Engineering, Royal Institute of Technology, Stockholm SE-100 44, Sweden*

[2] *Sandvik Coromant R&D, 126 80 Stockholm, Sweden*

[3] *Institute for Solid State Physics and Optics, Wigner Research Centre for Physics, H-1525 Budapest, Hungary*

[4] *Department of Physics and Astronomy, Division of Materials Theory, Uppsala University, SE-75120 Uppsala, Sweden*

(Received 6 September 2017; revised manuscript received 23 August 2018; published 13 December 2018)

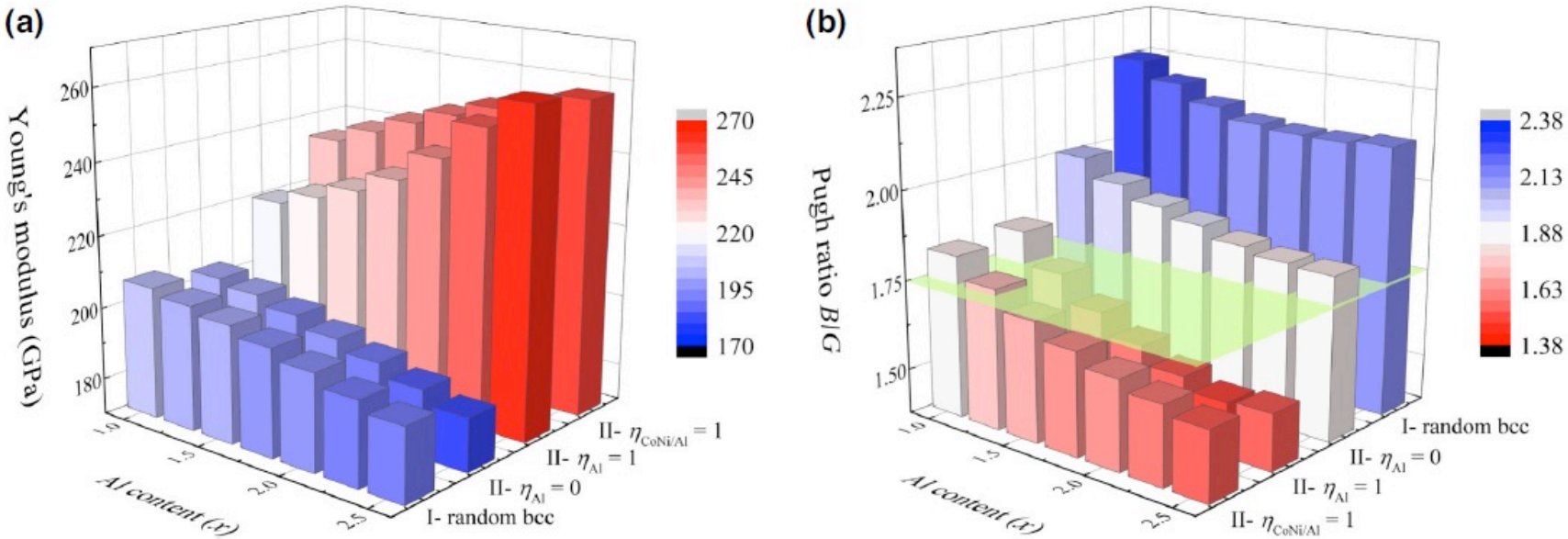

Binder phase in hard metals

Applied Materials Today 12 (2018) 322–329

Contents lists available at ScienceDirect

Applied Materials Today

journal homepage: www.elsevier.com/locate/apmt

High entropy alloys: Substituting for cobalt in cutting edge technology

Erik Holmström[a], Raquel Lizárraga[b,*], David Linder[b], Armin Salmasi[b], Wei Wang[b], Bartek Kaplan[a], Huahai Mao[c,b], Henrik Larsson[c,b], Levente Vitos[b,d,e]

[a] Sandvik Coromant R & D, SE-126 80 Stockholm, Sweden
[b] Department of Materials Science and Engineering, Royal Institute of Technology, Stockholm SE-100 44, Sweden
[c] Thermo-Calc Software AB, Råsundavägen 18, SE-169 67 Solna, Sweden
[d] Department of Physics and Astronomy, Division of Materials Theory, Uppsala University, Box 516, SE-75120 Uppsala, Sweden
[e] Institute for Solid State Physics and Optics, Wigner Research Centre for Physics, H-1525, P.O. Box 49, Hungary

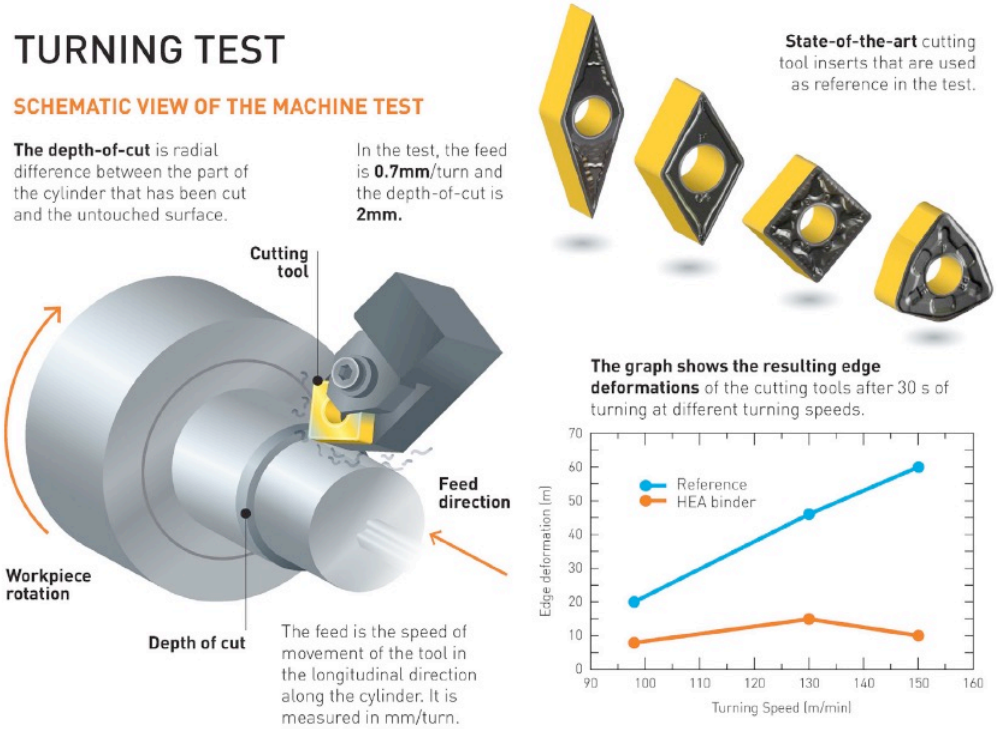

Fig. 5. A schematic view of the machine test, the results of the HEA bonded product compared to a state-of-the-art reference with Co as binder phase. The actual shape of the tested inserts is the third from the top.

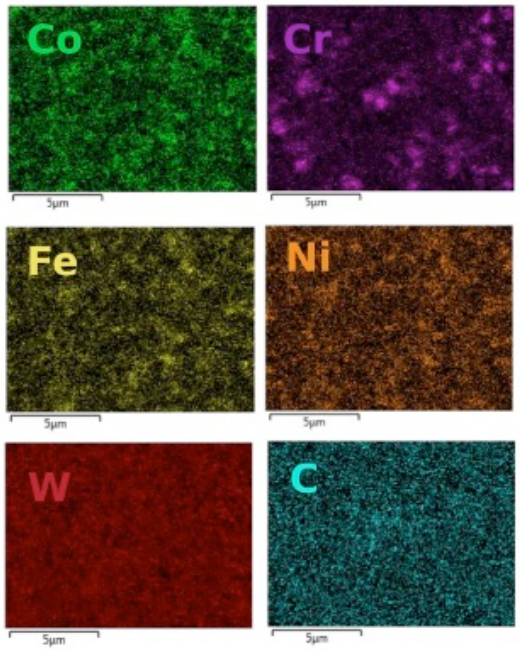

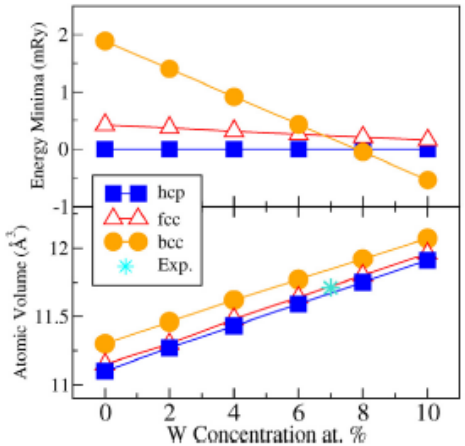

Plasticity, stacking fault energy of HEAs

Scripta Materialia 108 (2015) 44–47

Contents lists available at ScienceDirect

Scripta Materialia

journal homepage: www.elsevier.com/locate/scriptamat

Temperature dependent stacking fault energy of FeCrCoNiMn high entropy alloy

Shuo Huang [a,*], Wei Li [a], Song Lu [a], Fuyang Tian [b], Jiang Shen [b], Erik Holmström [c], Levente Vitos [a,d,e]

[a] Applied Materials Physics, Department of Materials Science and Engineering, Royal Institute of Technology, Stockholm SE-100 44, Sweden
[b] Department of Physics, University of Science and Technology Beijing, Beijing 100083, China
[c] Sandvik Coromant R&D, 126 80 Stockholm, Sweden
[d] Department of Physics and Astronomy, Division of Materials Theory, Uppsala University, Box 516, SE-75120 Uppsala, Sweden
[e] Institute for Solid State Physics and Optics, Wigner Research Centre for Physics, P.O. Box 49, H-1525 Budapest, Hungary

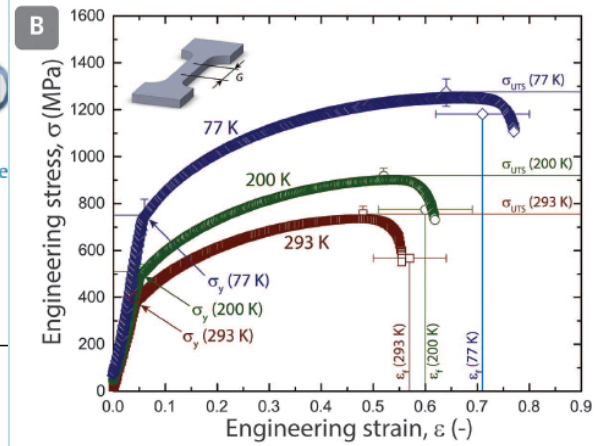

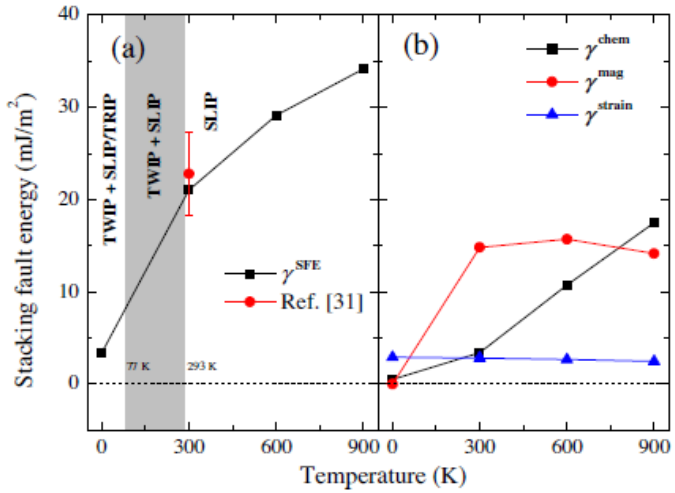

A fracture-resistant high-entropy alloy for cryogenic applications

Bernd Gludovatz,[1] Anton Hohenwarter,[2] Dhiraj Catoor,[3] Edwin H. Chang,[1] Easo P. George,[3,4*] Robert O. Ritchie[1,5*]

High-entropy alloys are equiatomic, multi-element systems that can crystallize as a single phase, despite containing multiple elements with different crystal structures. A rationale for this is that the configurational entropy contribution to the total free energy in alloys with five or more major elements may stabilize the solid-solution state relative to multiphase microstructures. We examined a five-element high-entropy alloy, CrMnFeCoNi, which forms a single-phase face-centered cubic solid solution, and found it to have exceptional damage tolerance with tensile strengths above 1 GPa and fracture toughness values exceeding 200 MPa·m$^{1/2}$. Furthermore, its mechanical properties actually improve at cryogenic temperatures; we attribute this to a transition from planar-slip dislocation activity at room temperature to deformation by mechanical nanotwinning with decreasing temperature, which results in continuous steady strain hardening.

Summary

(1) EMTO-CPA reproduces well the experimentally observed values and trends of the structural and mechanical properties of ordered and random systems

(2) special attention must be paid to the MT potential and single-site approximation

Important features:

- Localized MT orbitals (similar to the screened KKR)
- Smooth energy dependence of S(e,k)
- Optimized overlapping MT potential
- Proper normalization
- Accurate Full Charge Density
- Accurate kinetic and total energy